Geoscience Frontiers 11 (2020) 109–128

HOSTED BY

Contents lists available at ScienceDirect

China University of Geosciences (Beijing)

Geoscience Frontiers

journal homepage: www.elsevier.com/locate/gsf

Research Paper

Petrology of ultramafic to mafic cumulate rocks from the Göksun (Kahramanmaraş) ophiolite, southeast Turkey

Osman Parlak [a,b,*], Utku Bağcı [c], Tamer Rızaoğlu [d], Corina Ionescu [e,f], Güzide Önal [a], Volker Höck [g], Hüseyin Kozlu [h]

[a] Çukurova Üniversitesi, Jeoloji Mühendisliği Bölümü, Balcalı, TR-01330 Adana, Turkey
[b] State Key Laboratory of Geological Processes and Mineral Resources, Center for Global Tectonics, School of Earth Sciences, China University of Geosciences, Wuhan 430074, China
[c] Mersin Üniversitesi, Jeoloji Mühendisliği Bölümü, Çiftlikköy, TR-33343 Mersin, Turkey
[d] Kahramanmaraş Sütçü İmam Üniversitesi, Jeoloji Mühendisliği Bölümü, Avşar Kampüsü, TR-46100 Kahramanmaraş, Turkey
[e] Babeş-Bolyai University, Geology Department, 1 Kogălniceanu Str., RO-400084 Cluj-Napoca, Romania
[f] Kazan (Volga Region) Federal University, Archeotechnologies & Archeological Material Sciences Laboratory, 18 Kremlevskaya Str., 420000 Kazan, Russia
[g] University of Salzburg, Division of Geography and Geology, 34 Hellbrunner Str., A-5020 Salzburg, Austria
[h] Türkiye Petrolleri Anonim Ortaklığı, TR-06520 Ankara, Turkey

ARTICLE INFO

Article history:
Received 4 May 2018
Received in revised form
8 October 2018
Accepted 21 November 2018
Available online 10 January 2019

Keywords:
Göksun (Kahramanmaraş) ophiolite
Cumulate
SSZ-Spreading
Neotethys
Late Cretaceous
SE Anatolia

ABSTRACT

The Göksun (Kahramanmaraş) ophiolite (GKO), cropping out in a tectonic window bounded by the Malatya metamorphic unit on both the north and south, is located in the EW-trending lower nappe zone of the southeast Anatolian orogenic belt (Turkey). It exhibits a complete oceanic lithospheric section and overlies the Middle Eocene Maden Group/Complex with a tectonic contact at its base. The ophiolitic rocks and the tectonically overlying Malatya metamorphic (continental) unit were intruded by I-type calc-alkaline Late Cretaceous granitoid (~81–84 Ma). The ultramafic to cumulates in the GKO are represented by wehrlite, plagioclase wehrlite, olivine gabbro and gabbro. The crystallization order for the cumulate rocks is as follows: olivine ± chromian spinel → clinopyroxene → plagioclase. The major and trace element geochemistry as well as the mineral chemistry of the ultramafic to mafic cumulate rocks suggest that the primary magma generating the GKO is compositionally similar to that observed in the modern island-arc tholeiitic sequences. The mineral chemistry of the ultramafic to mafic cumulates indicates that they were derived from a mantle source that was previously depleted by earlier partial melting events. The highly magnesian olivine ($Fo_{77–83}$), clinopyroxene (Mg# of 82–90) and the highly Ca-plagioclase ($An_{81–89}$) exhibit a close similarity to those, which formed in a supra-subduction zone (SSZ) setting. The field and the geochemical evidence suggest that the GKO formed as part of a much larger sheet of oceanic lithosphere, which accreted to the base of the Tauride active continental margin, including the İspendere, Kömürhan and the Guleman ophiolites. The latter were contemporaneous and genetically/tectonically related within the same SSZ setting during the closure of the Neotethyan oceanic basin (Berit Ocean) between the Taurides to the north and the Bitlis-Pütürge massif to the south during the Late Cretaceous.

1. Introduction

The Late Cretaceous ophiolites in southeast Turkey play an important role in the tectonic evolution of the Bitlis-Zagros suture zone as well as in certain parts of the Alpine-Himalayan orogeny in a broader context. In general, the Neotethyan evolution of the southeast Anatolian suture began with rifting in the Triassic and ended with continental collision in the Miocene (Yılmaz, 1993;

* Corresponding author. Çukurova Üniversitesi, Jeoloji Mühendisliği Bölümü, Balcalı, TR-01330 Adana, Turkey. Fax: +90 322.338 67 15.
E-mail address: parlak@cu.edu.tr (O. Parlak).
Peer-review under responsibility of China University of Geosciences (Beijing).

https://doi.org/10.1016/j.gsf.2018.11.004

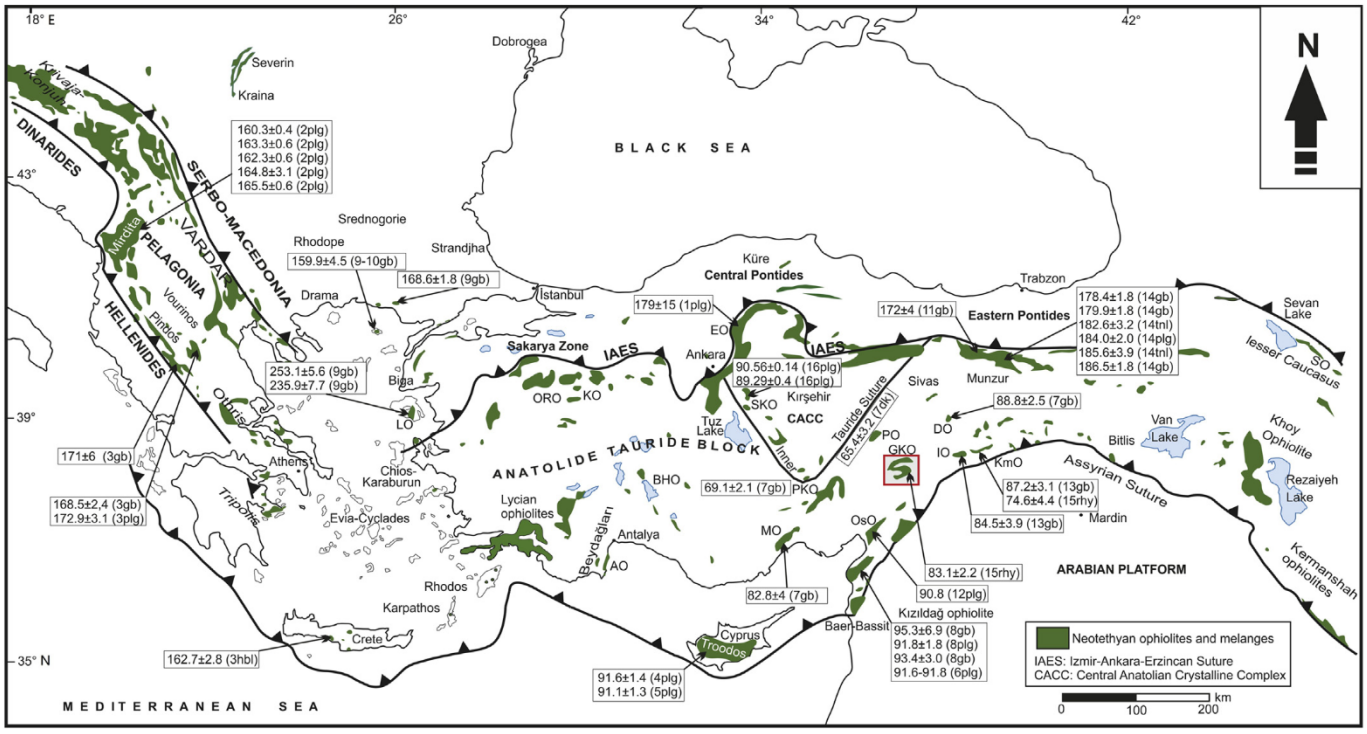

Figure 1. U-Pb ages of Tethyan ophiolites in Turkey and surrounding areas. Red box indicates the study area. Data are from (1) Dilek and Thy (2006), (2) Dilek et al. (2008), (3) Liati et al. (2004), (4) Mukasa and Ludden (1987), (5) Konstantinou et al. (2007), (6) Dilek and Thy (2009), (7) Parlak et al. (2013a), (8) Karaoğlan et al. (2013a), (9) Koglin (2008), (10) Koglin et al. (2009), (11) Topuz et al. (2012), (12) Sarıfakıoğlu et al. (2012), (13) Karaoğlan et al. (2012), (14) Robertson et al. (2013a), (15) Karaoğlan et al. (2013b), and (16) van Hinsbergen et al. (2016). Abbreviations for the ophiolitic complexes: LO—Lesvos, AO—Antalya, BHO—Beyşehir-Hoyran, ORO—Orhaneli, KO—Kınık, EO—Eldivan, MO—Mersin, PKO—Pozantı-Karsantı, OsO—Osmaniye, GKO—Göksun (Kahramanmaraş), PO—Pınarbaşı, IO—Ispendere, DO—Divriği, KmO—Kömürhan, SO—Sevan, SKO—Sarıkaraman. Abbreviations for rock types: plg—plagiogranite, gb—gabbro, dk—dyke, tnl—tonalite, rhy—rhyolite. The map is modified after Dilek and Flower (2003) and Çelik et al. (2011).

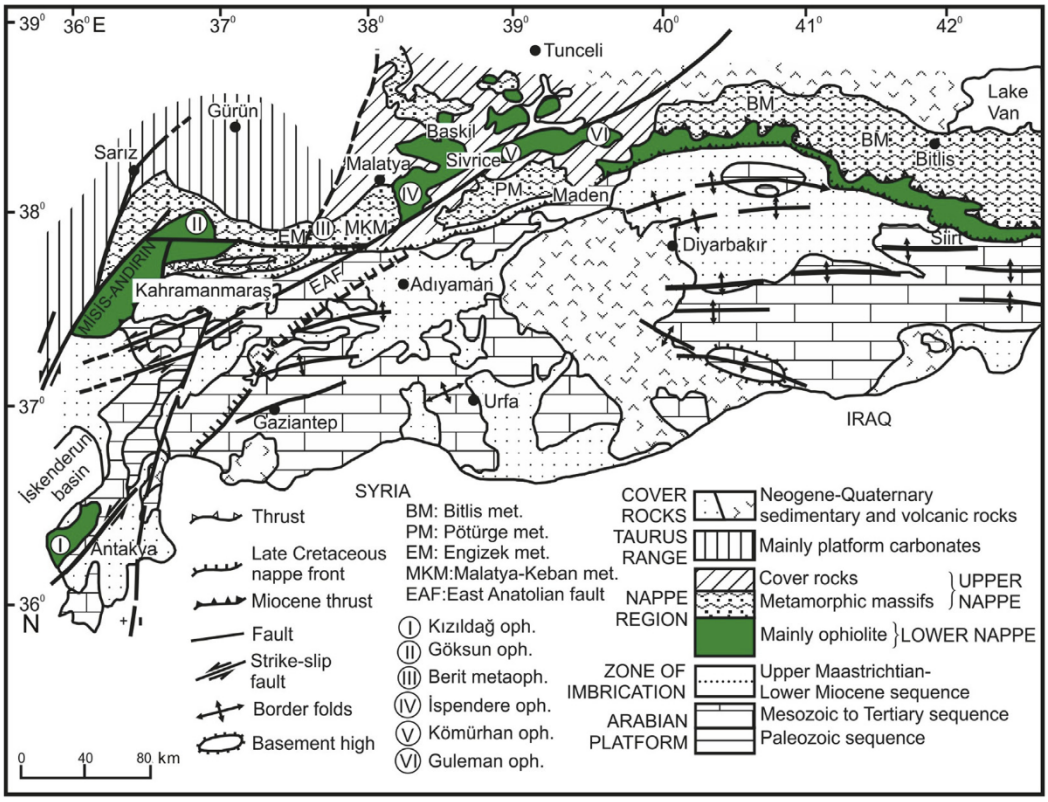

Figure 2. Main tectonic units and ophiolites of the southeast Anatolia (after Yılmaz et al., 1993). Abbreviations: met.—metamorphics, oph.—ophiolite, metaoph.—metaophiolite.

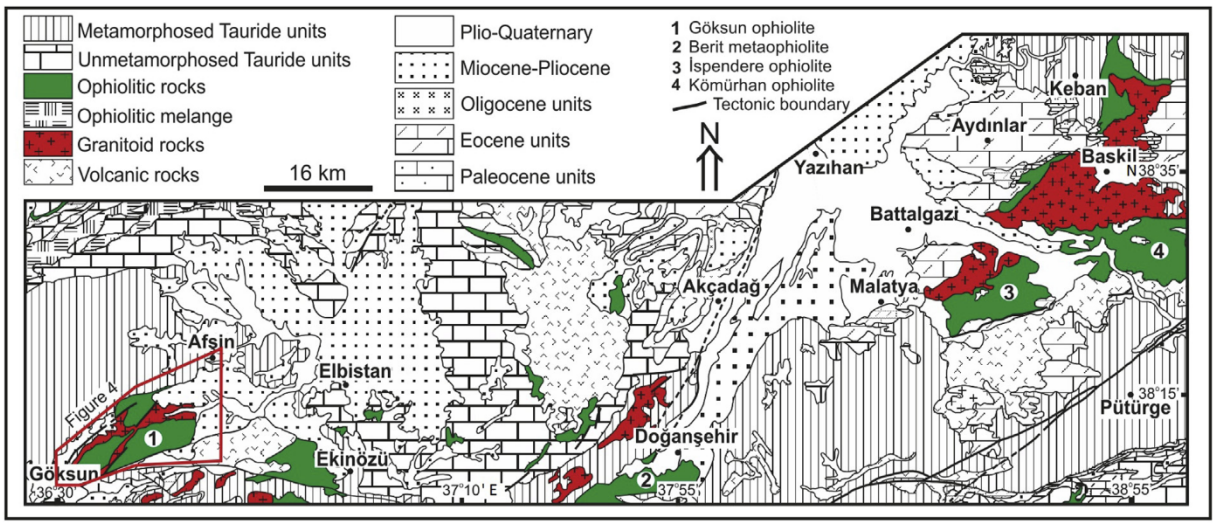

Figure 3. Simplified geological map of the area between Göksun (Kahramanmaraş) and Baskil (Elazığ), showing the distribution of ophiolites, granitoids and metamorphic massifs (MTA, 2002). The rectangle marks the area enlarged in Fig. 4.

Yılmaz et al., 1993; Robertson et al., 2006, 2007; Okay et al., 2010; Karaoğlan et al., 2016). The Late Cretaceous ophiolitic rocks form two subparallel belts, which transect southern Turkey, extending through northern Syria and Cyprus (Robertson, 2002; Parlak et al., 2009) (Figs. 1 and 2). The southern belt includes the Troodos ophiolite (Cyprus), the Baer–Bassit ophiolite (northern Syria), as well as the Antalya (Tekirova), the Kızıldağ (Hatay), the Amanos, and the Koçali ophiolites (southern Turkey) respectively. These ophiolites originated within the Southern Neotethys, between the Arabian platform to the south and the Bitlis and the Pütürge continental units to the north (Fig. 2). The more northerly belt includes the Göksun (Kahramanmaraş) ophiolite (GKO), the Berit metaophiolite, the İspendere ophiolite, the Kömürhan ophiolites and the Guleman ophiolite. These ophiolites originated from the Berit Ocean that was located between the Malatya-Keban platform, which is the southeast continuation of the Tauride platform to the north, and the Bitlis and Pütürge continental blocks to the south (Robertson et al., 2007, 2012, 2013b; Parlak et al., 2009).

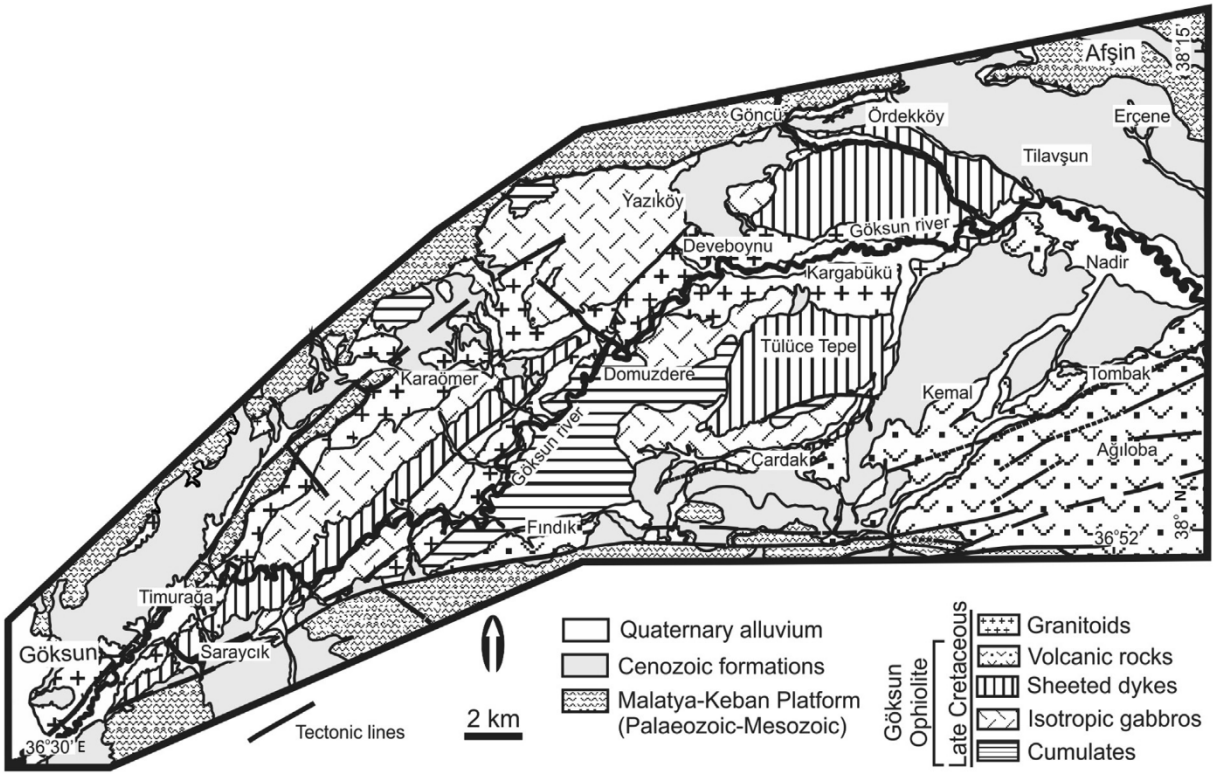

Figure 4. Detailed distribution of the Göksun (Kahramanmaraş) ophiolites in the Kahramanmaras area, between Göksun (SW) and Afşin (NE). Simplified geological map after Perinçek and Kozlu (1984) and Tarhan (1986).

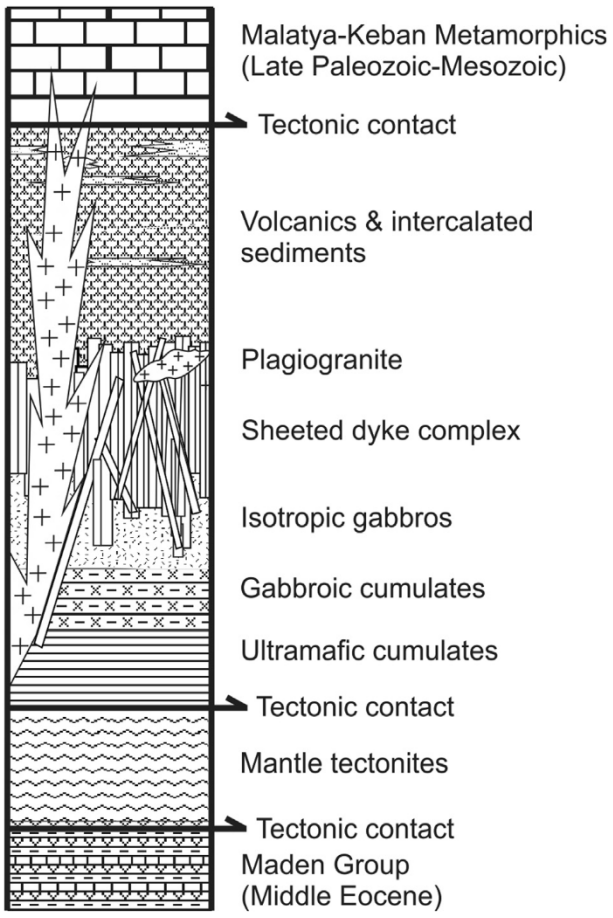

Figure 5. Synthetic log of the Göksun (Kahramanmaraş) ophiolite (modified after Parlak et al., 2004).

The ophiolites in the northern part of the Southeast Anatolian suture are tectonically attached to the Tauride (Malatya-Keban) platform and exhibit well-preserved oceanic lithospheric sections, from bottom to top, namely mantle tectonites, ultramafic to mafic cumulates, an isotropic gabbro, sheeted dykes with plagiogranite, and volcanic rocks. The volcanic section comprises rocks ranging from basalts to rhyolites, associated with tuffs and debris flows. It has been interpreted as an ensimatic island arc assemblage, built on a SSZ-type crust in Late Cretaceous (Parlak et al., 2004; Rızaoğlu et al., 2006; Robertson et al., 2007). The cumulate rocks have been widely used to designate the tectonic setting of ophiolites as well as magma chamber processes during the genesis of the oceanic crust along the Tethyan realm (Pallister and Hopson, 1981; Hébert and Laurent, 1990; Parlak et al., 1996, 2000, 2002, 2013b; Bağcı et al., 2005, 2006; Rızaoğlu et al., 2006; Saccani et al., 2013, 2014; Allahyari et al., 2014).

The aim of this paper is (i) to present the whole rock and mineral chemistry of the ultramafic to mafic cumulates from the GKO, (ii) to constrain their magma source, (iii) to show their genetic relations to upper crustal rocks, and (iv) to highlight the similarities of the studied rock units with other ophiolites of the Southeast Anatolian suture and from elsewhere in the Tethyan region.

2. Regional geology

The Southeast Anatolian orogen (SAO) is characterized by three distinct tectonic units, separated from one another by major, north dipping, thrust imbrications (Fig. 2). From north to south, the tectonic units are defined namely (i) the nappe zone, (ii) the zone of imbrication and (iii) the Arabian platform, respectively (Yılmaz, 1990, 1993; Yılmaz et al., 1993). The nappe zone in the north forms morphologically the highest tectonic unit and is divided into the lower and the upper nappe (Yılmaz, 1993). The lower nappe is characterized by mainly non-metamorphic to variably metamorphosed ophiolitic units, and the Maden Group/Complex. The upper nappe is represented by the Bitlis, the Pütürge, the Malatya,

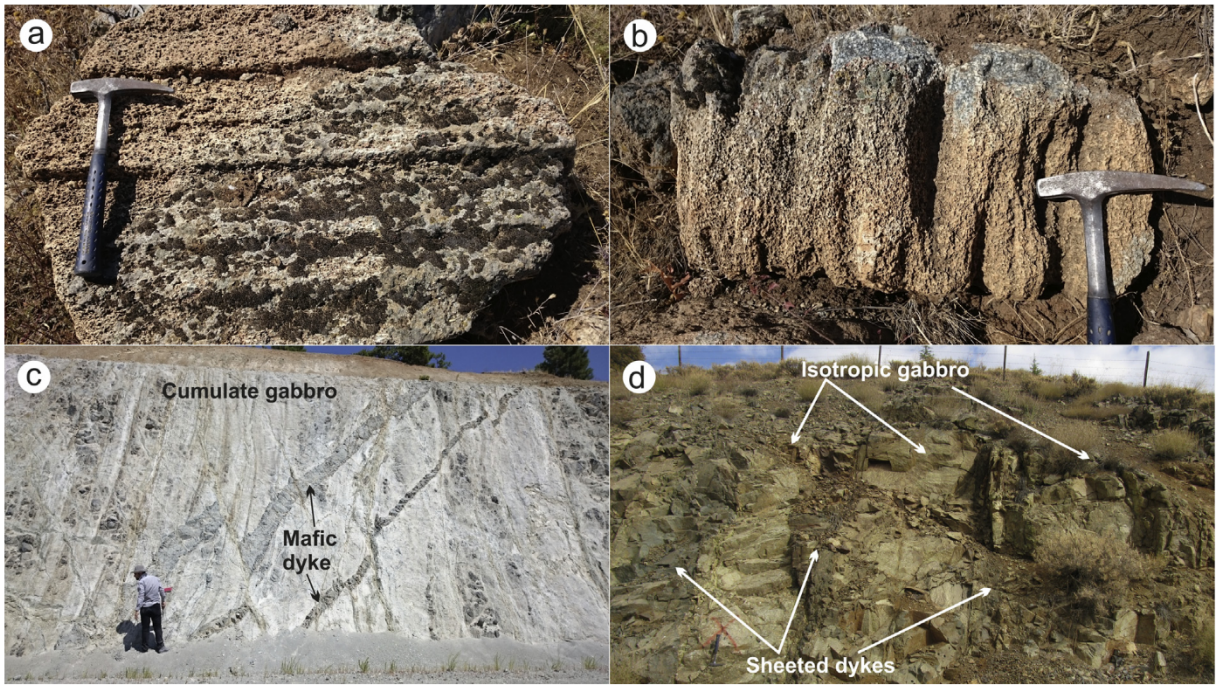

Figure 6. Field view of (a) cumulate gabbro intruded by mafic dykes, (b) banded gabbroic cumulate, (c) plagioclase bearing ultramafic cumulate and (d) isotropic gabbro-sheeted dyke transition zone.

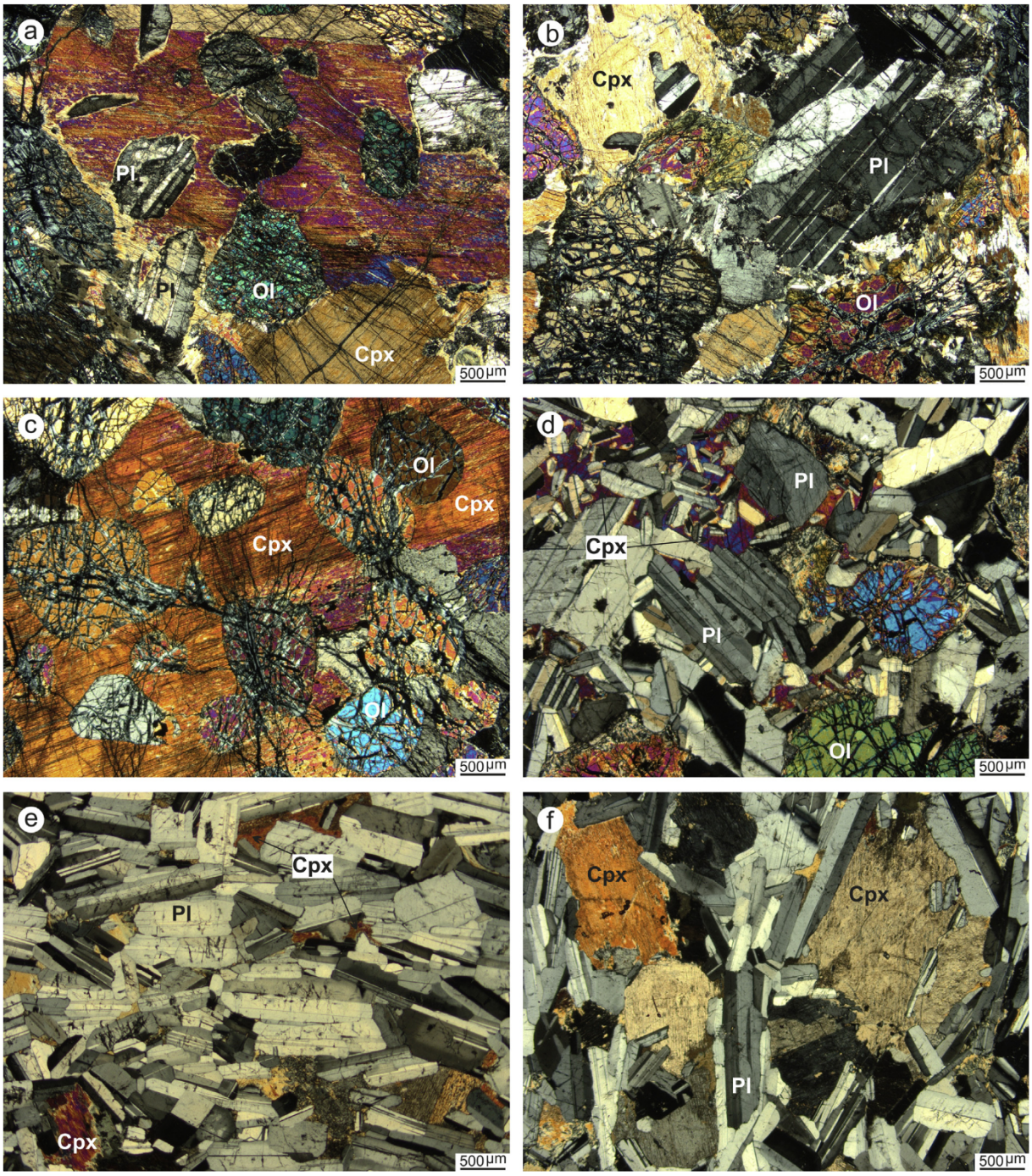

Figure 7. Photomicrographs of plagioclase wehrlite (a–b), poikilitic wehrlite (c), olivine gabbro (d) and gabbro (e–f). Abbreviations: Cpx–clinopyroxene, Ol–olivine, Pl–plagioclase.

the Keban, the Engizek and the Binboğa metamorphic (continental) massifs (Ketin, 1983; Yılmaz, 1993). The second tectonic unit, the zone of imbrication, forms a narrow, E–W trending belt, squeezed between the nappe region to the north and the Arabian platform to the south (Fig. 2). It is represented by several north dipping thrust slices with southern vergence (Yılmaz et al., 1987; Karig and Kozlu, 1990; Yılmaz, 1990). The rock units in the imbricated thrust slices range in age from Late Cretaceous to Early Miocene (Yılmaz, 1993). The last tectonic unit, the Arabian platform, comprises a Paleozoic–Mesozoic sequence overlying a Precambrian basement. The platform was overthrust from the north by ophiolites and various ophiolites-related units during latest Cretaceous time (Campanian–Maastrichtian), and was then unconformably overlain by a Cretaceous–Palaeogene non-marine to shallow marine succession. This was followed by the deposition of Lower Miocene turbidites that accumulated in a foredeep related to the final southward emplacement of the thrust belt in Mid-Miocene time (Baştuğ, 1980; Aktaş and Robertson, 1984; Dewey et al., 1986; Yılmaz, 1993).

The Late Cretaceous ophiolites from the lower nappe of the Southeast Anatolian Orogen are tectonically attached beneath the

Table 1
Whole rock XRF analyses of the ultramafic cumulate rocks of the Göksun (Kahramanmaraş) ophiolite. Major elements in wt.%, minor and trace elements in ppm. Fe^T as FeO*.

Samples	Ultramafic cumulates														
	Wehrlite										Plagioclase wehrlite				
	K-1	K-2	K-3	K-5	K-71	K-151	K-152	K-153	K-209	K-210	K-4	K-69	K-70	K-208	K-211
SiO_2	42.56	42.86	41.88	39.53	39.12	41.76	41.92	44.04	39.86	41.09	41.71	40.53	40.82	40.05	43.68
TiO_2	0.19	0.20	0.16	0.08	0.12	0.16	0.17	0.20	0.30	0.23	0.15	0.15	0.14	0.20	0.24
Al_2O_3	7.41	6.65	9.63	10.05	4.64	7.87	7.75	8.12	4.92	5.56	9.47	9.26	9.16	4.98	4.80
FeO*	11.58	11.89	10.75	11.76	14.59	12.07	12.11	10.02	11.07	10.50	11.09	11.83	11.81	11.51	11.80
Fe_2O_3					6.68							4.77	5.52		
FeO					7.91							7.06	6.29		
MnO	0.17	0.17	0.16	0.17	0.22	0.17	0.17	0.14	0.16	0.15	0.16	0.19	0.18	0.17	0.17
MgO	26.63	26.27	23.81	26.26	30.75	25.94	26.81	22.77	32.27	31.86	24.49	24.62	23.93	32.18	34.17
CaO	7.41	8.19	8.33	5.56	4.05	7.87	7.34	10.73	3.65	4.15	8.10	7.33	7.69	4.37	4.75
Na_2O	0.54	0.39	0.33	0.36	0.07	0.31	0.48	0.35	0.23	0.22	0.34	0.34	0.39	0.28	0.00
K_2O	0.05	0.03	0.03	0.03	0.00	0.02	0.04	0.02	0.03	0.04	0.03	0.01	0.00	0.02	0.01
P_2O_5	0.03	0.02	0.02	0.02	0.02	0.02	0.02	0.02	0.04	0.04	0.02	0.02	0.02	0.02	0.03
LOI	3.94	3.70	5.39	6.51	6.68	3.78	3.53	3.79	7.00	6.09	5.01	5.72	5.49	5.70	5.40
CO_2					0.18							0.16	0.20		
Cr_2O_3	0.12	0.11	0.09	0.02	0.11	0.10	0.15	0.15	0.46	0.39	0.10	0.05	0.07	0.48	0.48
NiO	0.11	0.12	0.09	0.09	0.18	0.13	0.14	0.09	0.20	0.18	0.09	0.10	0.10	0.21	0.17
Total	100.73	100.59	100.67	100.44	100.73	100.21	100.64	100.44	100.16	100.51	100.75	100.32	100.00	100.16	100.30
Nb	6	6	4	5	8	6	5	5	8	7	5	5	5	7	8
Zr	14	14	12	11	11	13	15	15	18	18	13	13	11	17	17
Y	14	15	13	12	14	7	8	9	15	11	13	14	13	10	11
Sr	30	30	54	54	16	43	41	39	29	33	50	49	43	23	24
U	2	2	2	2	2	2	2	2	2	2	2	2	2	2	2
Rb	12	10	10	10	10	2	4	4	3	2	11	9	11	3	3
Th	8	7	7	7	7	2	2	2	2	2	7	6	4	2	2
Pb	28	30	24	25	32	13	16	15	15	14	26	28	29	15	14
Ga	10	10	11	11	10	6	9	7	6	6	11	11	11	6	6
Ni	809	854	585	662	1107	842	803	557	1084	1026	622	672	678	1049	1054
Co	111	110	97	116	138	116	114	91	129	127	106	108	109	125	124
Cr	765	1359	1170	195	782	673	801	1058	2993	2638	1403	479	378	2723	3269
V	106	122	87	41	61	93	105	128	132	121	87	73	87	112	121
Ba	9	17	9	9	20	29	32	39	77	71	9	12	30	60	61
Hf	55	44	36	45	-	1	1	1	1	1	38	-	-	1	1
Sc	52	66	52	26	42	99	90	105	61	70	47	40	41	51	54

metamorphic Tauride platform units (Fig. 3). These ophiolites are represented, from west to east, by the Göksun (Kahramanmaraş) ophiolites, the Berit metaophiolite, the İspendere, the Kömürhan and the Guleman ophiolites (Fig. 3). Both the ophiolites and the metamorphic Tauride units were intruded by a number of I-type calc-alkaline Late Cretaceous to Eocene granitoids (Yazgan and Chessex, 1991; Parlak, 2006; Rızaoğlu et al., 2009; Kuşçu et al., 2010; Karaoğlan et al., 2013c, 2016) (Fig. 3).

The GKO is presently exposed in the area between Göksun and Afşin (Kahramanmaraş) (Fig. 4), within a tectonic window bounded by the Malatya metamorphic unit. It is characterized by a complete sequence composed, from bottom to top, of mantle tectonites, ultramafic-mafic cumulates, an isotropic gabbro, sheeted dike complex, plagiogranites and basic to acidic volcanic rocks (Parlak et al., 2004) (Fig. 5). The GKO has a tectonic contact with the Middle Eocene Maden Group/Complex and in turn is tectonically overlain by the Late Paleozoic–Mesozoic Malatya metamorphic unit (Perinçek and Kozlu, 1984; Parlak et al., 2004; Robertson et al., 2006) (Figs. 4 and 5). The contact between the mantle tectonites and the cumulates is also tectonic. In the study area, the ultramafic and mafic cumulates of the GKO crop out mainly between Fındık and Domuzdere. A small outcrop of cumulates can be seen west of Yazıköy (Fig. 4). These rocks display cumulate structures such as igneous lamination and rhythmic layering (Fig. 6a,b) and are intruded by mafic dykes (Fig. 6c). The contact with the isotropic gabbro is both tectonic and gradual. The isotropic gabbro is cut by individual dykes related to the sheeted dyke complex (Fig. 6d). The isotropic gabbro crops out in different parts of the study area, e.g. at Yazıköy, southwest of Karaöomer, and north of Çardak and Domuzdere. The isotropic gabbro gradually passes into the sheeted dykes. The volcanic rocks of the GKO crop out mainly in the east of area, around Çardak, Kemal, Tombak and Ağıloba (Fig. 4), although the contact relationships with the underlying units are obscured by Cenozoic units. The volcanic rocks are characterized by a wide-spectrum of rocks, ranging from basalt, basaltic andesite and andesite, to dacite and rhyolite (Parlak et al., 2004). The rhyolitic lava yields a zircon U-Pb age of 83.1 ± 2.2 Ma (Karaoğlan et al., 2013b). The sedimentary units covering the volcanic section comprise volcanogenic sandstone, tuff, agglomerate, mudstone and limestone. Late Cretaceous fossils from the cover or interbedded sediments, which were genetically related to the volcanic rocks, were reported by Perinçek and Kozlu (1984).

3. Petrography

The ultramafic cumulates in the GKO are represented by plagioclase wehrlite and wehrlite. Plagioclase wehrlite, exhibiting poikilitic texture, is composed of olivine (50%–55%), clinopyroxene (35%–40%), plagioclase (5%–10%) and orthopyroxene (2%–3%). Cumulus olivine crystals, with grain sizes between 0.3 mm and 3.3 mm are forsteritic in composition ($Fo_{77–81}$). Cumulus to post-cumulus clinopyroxene oikocrysts enclose olivines and plagioclases (Fig. 7a,b). Clinopyroxenes are diopsidic in composition ($En_{44–56}Fs_{6–11}Wo_{34–47}$). Subhedral to anhedral plagioclases are typically bytownitic in composition ($An_{87–89}$). They are present as not zoned cumulus grains with grain sizes between 0.7 mm and

Table 2
Whole rock XRF analyses of the mafic cumulate rocks of the Göksun (Kahramanmaraş) ophiolite. Major elements in wt.%, minor and trace elements in ppm. Fe^T as FeO*.

Sample	Mafic cumulates									
	Olivine gabbro	Gabbro								
	K-149	K-61	K-62	K-64	K-65	K-66	K-67	K-68	K-150	K-170
SiO_2	45.12	48.38	48.79	47.78	47.93	47.92	47.30	46.88	48.23	51.15
TiO_2	0.15	0.52	0.58	0.39	0.36	0.68	0.19	0.21	0.44	0.35
Al_2O_3	24.78	24.11	24.26	19.37	19.62	21.79	19.66	19.66	18.95	15.72
FeO*	4.20	4.62	4.06	5.26	6.20	5.62	4.88	4.56	4.66	8.27
Fe_2O_3		1.33	1.33	1.97	3.13	2.30	1.16	1.55		
FeO		3.29	2.73	3.29	3.07	3.32	3.72	3.01		
MnO	0.06	0.08	0.08	0.11	0.11	0.10	0.10	0.09	0.09	0.14
MgO	9.12	4.08	3.93	7.86	7.31	6.22	9.10	8.65	8.48	9.69
CaO	13.55	15.15	14.75	16.33	15.73	15.38	15.52	16.20	15.84	11.00
Na_2O	1.49	2.21	2.64	1.45	1.58	1.72	1.46	1.36	1.56	1.82
K_2O	0.02	0.01	0.04	0.01	0.00	0.02	0.00	0.00	0.04	0.19
P_2O_5	0.02	0.02	0.05	0.01	0.02	0.02	0.01	0.01	0.03	0.03
LOI	1.55	0.81	1.06	1.13	1.09	0.98	1.70	1.63	1.55	0.95
CO_2		0.10	0.00	0.25	0.00	0.12	0.16	0.19		
Cr_2O_3	0.09	0.04	0.04	0.12	0.09	0.04	0.12	0.13	0.24	0.13
NiO	0.06	0.01	0.01	0.01	0.01	0.01	0.02	0.02	0.06	0.03
Total	100.20	100.12	100.29	100.07	100.05	100.61	100.21	99.58	100.16	99.46
Nb	1	1	1	1	1	1	1	1	1	1
Zr	11	15	21	15	14	19	11	11	24	21
Y	6	10	12	12	13	12	11	11	15	14
Sr	130	184	191	123	138	148	143	139	147	85
U	2	2	2	4	3	2	3	2	2	2
Rb	2	2	2	4	3	3	5	4	2	6
Th	2	2	2	2	2	2	2	2	2	2
Pb	2	5	4	10	10	6	12	10	4	7
Ga	13	18	18	15	18	17	15	14	13	14
Ni	245	46	41	101	82	73	144	143	170	146
Co	37	21	16	31	31	29	41	35	27	42
Cr	214	261	260	735	586	281	706	780	1125	778
V	39	173	156	166	163	202	102	109	166	240
Ba	15	9	9	16	9	9	9	9	22	51
Hf	1	3	4	4	3	2	6	5	1	1
Sc	27	26	30	49	57	44	49	50	34	57

4.5 mm. The postcumulus orthopyroxenes are mainly enstatite ($En_{78-79}Fs_{17-18}Wo_{2-3}$).

Wehrlite exhibiting poikilitic texture, is composed of olivine (55–60 vol.%), clinopyroxene (35–40 vol.%) and orthopyroxene (1–2 vol.%). Cumulus olivine crystals with grain sizes between 0.4 mm and 2.8 mm are forsteritic in composition (Fo_{79-82}). Large cumulus to postcumulus clinopyroxenes poikilitically enclose olivines (Fig. 7c). Clinopyroxenes have a diopsidic ($En_{45-50}Fs_{5-11}Wo_{40-49}$) and orthopyroxene an enstatitic ($En_{79}Fs_{18}Wo_3$) composition. Some of clinopyroxenes are transformed into brown amphibole.

The mafic cumulates in the GKO consist of olivine gabbro and gabbro. The first one shows mesocumulate to orthocumulate textures and is composed of 60–70 vol.% bytownitic plagioclase (An_{81-87}), 15–20 vol.% forsteritic olivine (Fo_{82-83}), 7–10 vol.% diopsidic clinopyroxene ($En_{45-50}Fs_{6-9}Wo_{41-47}$) and ~1 vol.% enstatitic orthopyroxene ($En_{81}Fs_{17}Wo_3$) (Fig. 7d). Plagioclases are present as unzoned cumulus grains with grain sizes between 0.7 mm and 3 mm. Euhedral to subhedral olivine with grain sizes between 0.9 mm and 3.2 mm forms the cumulus phase. Anhedral clinopyroxenes are observed as cumulus to intercumulus phases, enclosing plagioclase (Fig. 7d). Also orthopyroxene is present as intercumulus phase.

Gabbro displays an adcumulate texture, represented by planar lamination of tabular plagioclase and postcumulus clinopyroxene and orthopyroxene (Fig. 7e). It is composed of plagioclase (65–70 vol.%), clinopyroxene (20–40 vol.%) and orthopyroxene (2–3 vol.%). Plagioclases are labradorite to bytownite in composition (An_{65-84}) (Table 5), have grain sizes between 0.4 mm and 2.4 mm and show zoning. Anhedral clinopyroxenes with diopside composition ($En_{44-55}Fs_{6-11}Wo_{34-47}$) are observed as intercumulus phases, sometimes poikilitically enclosing plagioclase (Fig. 7f). Some of clinopyroxenes are transformed to amphibole. Based on the petrographic observations, the crystallization order within the cumulate rocks of the GKO is olivine ± chromian spinel → clinopyroxene → plagioclase.

4. Analytical methods

A total of 25 selected samples (15 ultramafic cumulates and 10 mafic cumulates) were analyzed for major and trace elements by X-ray fluorescence spectrometry (XRF) in the Mineralogy Department at the University of Geneva. Major element contents were determined on glass beads fused at 1150 °C in a gold–platinum crucible. The glass beads were obtained by melting powdered sample with $Li_2B_4O_7$ was added at a ratio of 1:5. Trace element contents were measured on pressed-powder pellets. The results of whole rock chemical analyses are presented in Tables 1 and 2.

For microchemical analysis three hundred and seventy-one points from ten carbon-coated polished thin sections of ultramafic and mafic cumulate rocks, were analyzed with a JXA Superprobe 8600 electron microprobe (EMP) equipped with four wavelength dispersive spectrometers (WDS) and one Si(Li) energy-dispersive spectrometer (EDS), at the Division Geography and Geology at Salzburg University (Austria). The analytical conditions for the elements were 13 s (20 s for peak and 10 s for background) of

Table 3
Representative EMP analyses of major elements (in wt.%) in olivines from the cumulate rocks of the Göksun (Kahramanmaraş) ophiolite. Calculations on 4 O basis according to Deer et al. (1992).

Sample	Ultramafic cumulates														Mafic cumulates			
	Plagioclase wehrlite								Wehrlite						Olivine gabbro			
	K4-3c	K4-5c	K4-10c	K69-2c	K69-11c	K70-4c	K70-12c	K70-19c	K71-2c	K71-5c	K71-8c	K153-1c	K153-14c	K153-15c	K149-9c	K149-21c	K149-21r	K149-22c
SiO_2	38.90	39.40	39.60	38.10	38.90	38.90	38.90	38.90	39.20	39.20	39.70	39.20	39.10	39.50	39.60	39.80	39.70	39.80
TiO_2	0.00	0.00	0.00	0.00	0.00	0.00	0.00	0.00	0.00	0.00	0.05	0.00	0.00	0.00	0.00	0.00	0.00	0.00
Al_2O_3	0.00	0.00	0.08	0.00	0.00	0.00	0.00	0.00	0.02	0.00	0.02	0.00	0.00	0.00	0.00	0.00	0.00	0.00
FeO*	18.50	18.30	17.80	20.90	19.40	19.50	19.80	20.60	18.80	19.30	18.60	18.80	18.00	17.20	16.60	16.40	16.30	16.00
Cr_2O_3	0.00	0.00	0.00	0.00	0.00	0.00	0.00	0.00	0.00	0.00	0.00	0.00	0.00	0.00	0.00	0.00	0.00	0.00
MnO	0.28	0.26	0.28	0.34	0.32	0.27	0.31	0.30	0.29	0.29	0.29	0.26	0.28	0.27	0.27	0.26	0.24	0.24
MgO	42.00	42.20	42.10	40.10	41.50	41.80	41.10	40.70	41.90	41.80	42.20	42.50	43.00	43.60	43.50	44.00	44.40	44.00
CaO	0.15	0.12	0.49	0.02	0.04	0.04	0.00	0.03	0.04	0.06	0.03	0.16	0.20	0.21	0.10	0.12	0.08	0.10
Na_2O	0.00	0.00	0.00	0.00	0.00	0.00	0.00	0.00	0.00	0.00	0.00	0.00	0.00	0.00	0.00	0.00	0.00	0.00
K_2O	0.00	0.00	0.00	0.00	0.00	0.02	0.00	0.00	0.00	0.00	0.00	0.00	0.00	0.00	0.00	0.00	0.00	0.00
NiO	0.23	0.27	0.19	0.18	0.16	0.14	0.16	0.22	0.17	0.23	0.19	0.26	0.27	0.18	0.20	0.18	0.20	0.15
Total	100.06	100.55	100.54	99.64	100.32	100.67	100.27	100.75	100.42	100.88	101.08	101.18	100.85	100.96	100.27	100.76	100.92	100.29
Si	0.99	1.00	1.00	0.99	1.00	0.99	1.00	1.00	1.00	1.00	1.00	0.99	0.99	0.99	1.00	1.00	0.99	1.00
Ti	0.00	0.00	0.00	0.00	0.00	0.00	0.00	0.00	0.00	0.00	0.00	0.00	0.00	0.00	0.00	0.00	0.00	0.00
Al	0.00	0.00	0.00	0.00	0.00	0.00	0.00	0.00	0.00	0.00	0.00	0.00	0.00	0.00	0.00	0.00	0.00	0.00
Fe	0.40	0.39	0.38	0.45	0.42	0.42	0.42	0.44	0.40	0.41	0.39	0.40	0.38	0.36	0.35	0.34	0.34	0.34
Cr	0.00	0.00	0.00	0.00	0.00	0.00	0.00	0.00	0.00	0.00	0.00	0.00	0.00	0.00	0.00	0.00	0.00	0.00
Mn	0.01	0.01	0.01	0.01	0.01	0.01	0.01	0.01	0.01	0.01	0.01	0.01	0.01	0.01	0.01	0.01	0.01	0.01
Mg	1.60	1.60	1.59	1.55	1.58	1.59	1.57	1.55	1.59	1.58	1.59	1.60	1.62	1.64	1.64	1.65	1.66	1.65
Ca	0.00	0.00	0.01	0.00	0.00	0.00	0.00	0.00	0.00	0.00	0.00	0.00	0.01	0.01	0.00	0.00	0.00	0.00
Na	0.00	0.00	0.00	0.00	0.00	0.00	0.00	0.00	0.00	0.00	0.00	0.00	0.00	0.00	0.00	0.00	0.00	0.00
K	0.00	0.00	0.00	0.00	0.00	0.00	0.00	0.00	0.00	0.00	0.00	0.00	0.00	0.00	0.00	0.00	0.00	0.00
Ni	0.01	0.01	0.01	0.00	0.00	0.00	0.00	0.00	0.00	0.00	0.00	0.01	0.01	0.01	0.01	0.01	0.01	0.01
Total	3.01	3.01	3.00	3.01	3.00	3.01	3.00	3.00	3.00	3.00	3.00	3.01	3.02	3.01	3.00	3.00	3.01	3.00
Fo	80.19	80.44	80.83	77.38	79.23	79.26	78.73	77.89	79.89	79.43	80.18	80.12	80.99	81.88	82.37	82.71	82.92	83.06
Fa	19.81	19.56	19.17	22.62	20.77	20.74	21.27	22.11	20.11	20.57	19.82	19.88	19.01	18.12	17.63	17.29	17.08	16.94
Mg#	79.95	80.21	80.59	77.09	78.95	79.03	78.46	77.64	79.64	79.18	79.93	79.90	80.74	81.65	82.13	82.48	82.71	82.85

Total Fe is expressed as FeO*.
c and r represent core and rim respectively.

Table 4
Representative EMP analyses of major elements (in wt.%) in clinopyroxenes from the cumulate rocks of the Göksun (Kahramanmaraş) ophiolite. Calculations on 6 O basis according to Deer et al. (1992).

Sample	Ultramafic cumulates										Mafic cumulates									
	Plagioclase wehrlite						Wehrlite				Olivine gabbro		Gabbro							
	K4-13c	K4-14c	K69-7c	K69-11c	K70-14c	K70-15c	K71-3c	K71-5c	K153-1c	K153-12c	K149-1c	K149-21c	K61-12c	K61-12r	K62-8c	K62-19c	K64-17c	K64-18c	K66-7c	K66-19c
SiO_2	52.60	52.20	52.90	51.40	53.90	52.10	52.90	52.50	54.50	52.70	53.30	52.60	52.90	52.60	51.40	51.20	52.40	51.50	51.80	51.00
Al_2O_3	2.80	2.57	2.66	2.37	1.30	2.45	2.50	2.73	0.66	2.21	1.56	2.45	2.57	1.55	2.45	3.21	2.55	2.60	2.27	2.52
TiO_2	0.37	0.56	0.33	0.35	0.13	0.88	0.46	0.43	0.12	0.40	0.61	0.76	0.44	0.42	0.78	0.47	0.41	0.71	0.44	0.92
FeO*	4.40	5.90	3.80	6.10	4.50	6.20	6.80	5.00	3.40	5.90	3.90	5.30	5.30	8.40	9.40	6.10	6.20	8.50	6.80	8.10
MnO	0.17	0.17	0.11	0.27	0.15	0.15	0.17	0.15	0.12	0.11	0.14	0.17	0.13	0.25	0.29	0.16	0.16	0.23	0.17	0.24
MgO	16.90	16.60	17.20	16.10	16.50	15.90	17.20	16.10	16.80	16.70	17.00	16.70	16.60	14.80	14.00	16.30	16.50	15.30	15.90	13.80
Cr_2O_3	0.97	0.66	0.73	0.29	0.40	0.28	0.70	0.90	0.12	0.13	0.29	0.32	0.28	0.27	0.20	0.22	0.36	0.38	0.23	0.08
CaO	22.10	21.40	22.40	21.20	23.50	21.20	19.40	22.10	25.40	21.50	23.30	21.70	21.50	21.70	21.30	21.50	21.10	20.30	21.00	22.10
Na_2O	0.18	0.30	0.25	0.25	0.21	0.34	0.33	0.40	0.00	0.22	0.22	0.27	0.21	0.27	0.33	0.24	0.27	0.35	0.25	0.33
K_2O	0.00	0.00	0.00	0.00	0.00	0.00	0.00	0.02	0.00	0.00	0.00	0.00	0.00	0.00	0.00	0.00	0.00	0.00	0.00	0.00
NiO	0.00	0.00	0.00	0.00	0.00	0.00	0.00	0.07	0.00	0.00	0.00	0.00	0.00	0.00	0.00	0.00	0.06	0.00	0.00	0.00
Total	100.49	100.36	100.38	98.33	100.59	99.50	100.46	100.40	101.12	99.87	100.32	100.27	99.93	100.26	100.15	99.40	100.01	99.87	98.86	99.09
Si	1.91	1.91	1.92	1.92	1.96	1.93	1.93	1.92	1.97	1.93	1.94	1.92	1.94	1.95	1.91	1.89	1.92	1.91	1.93	1.91
Al^{IV}	0.09	0.09	0.08	0.08	0.04	0.07	0.07	0.08	0.03	0.07	0.06	0.08	0.06	0.05	0.09	0.11	0.08	0.09	0.07	0.09
Al^{VI}	0.03	0.02	0.03	0.02	0.02	0.03	0.04	0.03	0.00	0.03	0.01	0.03	0.05	0.02	0.02	0.03	0.03	0.02	0.03	0.03
Ti	0.01	0.02	0.01	0.01	0.00	0.02	0.01	0.01	0.00	0.01	0.02	0.02	0.01	0.01	0.02	0.01	0.01	0.02	0.01	0.03
Fe^{3+}	0.02	0.05	0.03	0.05	0.02	0.01	0.01	0.03	0.02	0.03	0.03	0.02	0.00	0.03	0.04	0.07	0.03	0.04	0.03	0.03
Fe^{2+}	0.12	0.13	0.09	0.14	0.12	0.18	0.20	0.12	0.08	0.15	0.09	0.14	0.17	0.23	0.25	0.12	0.16	0.22	0.18	0.22
Mn	0.01	0.01	0.00	0.01	0.00	0.00	0.01	0.00	0.00	0.00	0.00	0.01	0.00	0.01	0.01	0.00	0.00	0.01	0.01	0.01
Mg	0.92	0.90	0.93	0.90	0.90	0.88	0.94	0.88	0.91	0.91	0.92	0.91	0.91	0.82	0.78	0.90	0.90	0.85	0.88	0.77
Cr	0.03	0.02	0.02	0.01	0.01	0.01	0.02	0.03	0.00	0.00	0.01	0.01	0.01	0.01	0.01	0.01	0.01	0.01	0.01	0.00
Ca	0.86	0.84	0.87	0.85	0.92	0.84	0.76	0.86	0.98	0.84	0.91	0.85	0.84	0.86	0.85	0.85	0.83	0.81	0.84	0.89
Na	0.01	0.02	0.02	0.02	0.01	0.02	0.02	0.03	0.00	0.02	0.02	0.02	0.01	0.02	0.02	0.02	0.02	0.03	0.02	0.02
K	0.00	0.00	0.00	0.00	0.00	0.00	0.00	0.00	0.00	0.00	0.00	0.00	0.00	0.00	0.00	0.00	0.00	0.00	0.00	0.00
Ni	0.00	0.00	0.00	0.00	0.00	0.00	0.00	0.00	0.00	0.00	0.00	0.00	0.00	0.00	0.00	0.00	0.00	0.00	0.00	0.00
Total	4.00	4.00	4.00	4.00	4.00	4.00	4.00	4.00	4.00	4.00	4.00	4.00	4.00	4.00	4.00	4.00	4.00	4.00	4.00	4.00
En	47.81	46.91	48.46	46.12	45.84	45.82	49.07	46.17	45.37	47.01	47.21	47.22	47.30	41.99	40.30	46.22	46.83	43.98	45.56	40.16
Fs	7.26	9.63	6.18	10.24	7.25	10.27	11.16	8.29	5.33	9.49	6.30	8.68	8.68	13.77	15.65	9.96	10.13	14.08	11.20	13.62
Wo	44.93	43.46	45.36	43.64	46.91	43.91	39.77	45.54	49.29	43.49	46.50	44.10	44.02	44.24	44.06	43.81	43.04	41.94	43.24	46.22
Total	100.00	100.00	100.00	100.00	100.00	100.00	100.00	100.00	100.00	100.00	100.00	100.00	100.00	100.00	100.00	100.00	100.00	100.00	100.00	100.00
Mg#	87.26	83.38	88.97	82.47	86.73	82.05	81.85	85.17	89.81	83.46	88.60	84.89	84.81	75.85	72.64	82.65	82.59	76.24	80.65	75.23

Total Fe is expressed as FeO*.
c and r represent core and rim respectively.

Table 5
Representative EMP analyses of major elements (in wt.%) in plagioclases from the cumulate rocks of the Göksun (Kahramanmaraş) ophiolite. Calculations on 16 O basis according to Deer et al. (1992).

Sample	Ultramafic cumulates				Mafic cumulates														
	Pl-Wehrlite			Wehrlite	Ol-Gabbro		Gabbro												
	K4-1c	K4-2c	K4-3c	K71-1c	K149-4c	K149-22c	K61-1c	K61-1r	K61-4c	K61-4r	K62-8c	K62-12c	K64-7c	K64-14c	K66-1c	K66-1r	K66-2c	K66-2r	K66-10c
SiO_2	45.60	45.50	45.70	46.84	47.50	46.00	47.80	51.00	48.30	50.70	50.70	47.80	47.20	49.30	47.90	50.10	48.30	51.10	47.10
Al_2O_3	33.70	33.60	34.20	33.96	32.80	33.80	33.10	31.20	33.00	31.40	31.50	33.40	33.80	32.30	33.20	31.70	33.30	31.10	33.80
TiO_2	0.00	0.00	0.00	0.00	0.00	0.00	0.00	0.00	0.00	0.00	0.00	0.00	0.00	0.00	0.00	0.00	0.00	0.00	0.00
FeO*	0.48	0.45	0.57	0.22	0.49	0.40	0.36	0.37	0.42	0.37	0.37	0.42	0.45	0.44	0.43	0.50	0.35	0.38	0.39
MnO	0.00	0.00	0.00	0.00	0.00	0.00	0.00	0.00	0.00	0.00	0.00	0.00	0.00	0.00	0.00	0.00	0.00	0.00	0.00
MgO	0.06	0.03	0.00	0.00	0.07	0.05	0.00	0.03	0.03	0.04	0.03	0.00	0.03	0.04	0.02	0.06	0.00	0.02	0.00
CaO	17.90	18.50	18.20	17.18	16.60	17.80	16.60	14.00	16.30	14.40	14.30	16.60	17.00	15.40	16.60	14.60	16.50	14.00	17.10
Na_2O	1.43	1.24	1.30	1.83	2.09	1.53	2.04	3.57	2.32	3.43	3.45	2.04	1.86	2.86	2.15	3.26	2.21	3.63	1.83
K_2O	0.00	0.00	0.00	0.00	0.03	0.00	0.00	0.03	0.00	0.02	0.07	0.02	0.02	0.02	0.03	0.05	0.02	0.03	0.02
Total	99.17	99.32	99.97	100.03	99.58	99.58	99.90	100.20	100.37	100.36	100.42	100.28	100.36	100.36	100.33	100.27	100.68	100.26	100.24
Si	2.12	2.11	2.11	2.15	2.19	2.12	2.20	2.32	2.20	2.30	2.30	2.19	2.16	2.24	2.19	2.28	2.20	2.32	2.16
Al^{IV}	0.88	0.89	0.89	0.85	0.81	0.88	0.80	0.68	0.80	0.70	0.70	0.81	0.84	0.76	0.81	0.72	0.80	0.68	0.84
Al^{VI}	0.96	0.95	0.96	0.98	0.97	0.96	0.99	0.99	0.98	0.98	0.98	0.99	0.98	0.98	0.98	0.98	0.99	0.98	0.98
Ti	0.00	0.00	0.00	0.00	0.00	0.00	0.00	0.00	0.00	0.00	0.00	0.00	0.00	0.00	0.00	0.00	0.00	0.00	0.00
Fe^{2+}	0.02	0.02	0.02	0.01	0.02	0.02	0.01	0.01	0.02	0.01	0.01	0.02	0.02	0.02	0.02	0.02	0.01	0.01	0.01
Mn	0.00	0.00	0.00	0.00	0.00	0.00	0.00	0.00	0.00	0.00	0.00	0.00	0.00	0.00	0.00	0.00	0.00	0.00	0.00
Mg	0.00	0.00	0.00	0.00	0.00	0.00	0.00	0.00	0.00	0.00	0.00	0.00	0.00	0.00	0.00	0.00	0.00	0.00	0.00
Ca	0.89	0.92	0.90	0.84	0.82	0.88	0.82	0.68	0.80	0.70	0.69	0.81	0.83	0.75	0.81	0.71	0.80	0.68	0.84
Na	0.13	0.11	0.12	0.16	0.19	0.14	0.18	0.31	0.21	0.30	0.30	0.18	0.16	0.25	0.19	0.29	0.20	0.32	0.16
K	0.00	0.00	0.00	0.00	0.00	0.00	0.00	0.00	0.00	0.00	0.00	0.00	0.00	0.00	0.00	0.00	0.00	0.00	0.00
Total	5.00	5.00	5.00	5.00	5.00	5.00	5.00	5.00	5.00	5.00	5.00	5.00	5.00	5.00	5.00	5.00	5.00	5.00	5.00
Or	0.00	0.00	0.00	0.00	0.17	0.00	0.00	0.17	0.00	0.12	0.40	0.12	0.12	0.12	0.17	0.29	0.12	0.17	0.12
Ab	12.63	10.82	11.45	16.16	18.52	13.46	18.19	31.52	20.48	30.09	30.27	18.17	16.51	25.12	18.95	28.69	19.49	31.88	16.21
An	87.37	89.18	88.55	83.84	81.30	86.54	81.81	68.31	79.52	69.80	69.33	81.71	83.38	74.76	80.87	71.02	80.40	67.95	83.68

Total Fe is expressed as FeO*.
c and r represent core and rim respectively.

Table 6
Representative EMP analyses of major elements (in wt.%) in orthopyroxenes from the cumulate rocks of the Göksun (Kahramanmaraş) ophiolite. Calculations on 6 O basis according to Deer et al. (1992).

Sample	Ultramafic cumulate					Mafic cumulate
	Pl-Wehrlite				Wehrlite	Ol-Gabbro
	K4-6c	K4-10c	K4-15c	K4-16c	K153-10c	K149-7c
SiO_2	54.70	54.90	55.10	55.10	54.70	54.80
Al_2O_3	1.42	1.39	1.35	1.40	1.26	1.55
TiO_2	0.65	0.38	0.61	0.39	0.63	0.60
FeO*	12.00	11.60	12.10	11.90	11.90	10.80
MnO	0.33	0.27	0.28	0.30	0.26	0.30
MgO	29.20	29.20	29.20	29.50	29.40	30.20
Cr_2O_3	0.00	0.00	0.00	0.00	0.00	0.22
CaO	1.58	1.63	1.31	1.59	1.48	1.45
Na_2O	0.00	0.00	0.00	0.00	0.00	0.00
K_2O	0.00	0.00	0.00	0.00	0.00	0.00
NiO	0.11	0.00	0.00	0.00	0.00	0.00
Total	99.99	99.37	99.95	100.18	99.63	99.92
Si	1.95	1.96	1.96	1.95	1.95	1.94
Al^{IV}	0.05	0.04	0.04	0.05	0.05	0.06
Al^{VI}	0.00	0.02	0.02	0.01	0.00	0.00
Ti	0.02	0.01	0.02	0.01	0.02	0.02
Fe^{3+}	0.02	0.00	−0.01	0.02	0.01	0.02
Fe^{2+}	0.34	0.35	0.37	0.33	0.34	0.30
Mn	0.01	0.01	0.01	0.01	0.01	0.01
Mg	1.55	1.55	1.55	1.56	1.56	1.59
Cr	0.00	0.00	0.00	0.00	0.00	0.01
Ca	0.06	0.06	0.05	0.06	0.06	0.05
Na	0.00	0.00	0.00	0.00	0.00	0.00
K	0.00	0.00	0.00	0.00	0.00	0.00
Ni	0.00	0.00	0.00	0.00	0.00	0.00
Total	4.00	4.00	4.00	4.00	4.00	4.00
En	78.38	78.85	78.73	78.69	78.85	80.60
Fs	18.57	17.98	18.73	18.26	18.30	16.62
Wo	3.05	3.16	2.54	3.05	2.85	2.78
Total	100.00	100.00	100.00	100.00	100.00	100.00

Total Fe is expressed as FeO*.
c and r represent core and rim respectively.

counting interval, ≤5 μm electron-beam diameter, accelerating voltage of 15 kV, beam current of 20 nA for backscattered electron (BSE) image capture and 40 nA for quantitative analysis. The standards used were: quartz for Si, synthetic γ-Al_2O_3 for Al, synthetic FeO for Fe, rutile for Ti, apatite for Ca and P, synthetic periclase for Mg, halite for Na, sylvite for K, MnO for Mn, Cr_2O_3 for Cr and metallic Ni for Ni. The detection limits were 0.05 wt.% for SiO_2, 0.04 wt.% for TiO_2, 0.06 wt.% for FeO, Cr_2O_3 and NiO, 0.03 wt.% for Al_2O_3 and MnO, 0.02 wt.% for MgO, CaO, Na_2O and K_2O, and 0.07 wt.% for P_2O_5. The analytical error was 0.5%–1% at high concentrations, 5%–10% at low concentrations and ~30% close to the detection limit. The calculation of the chemical composition follows the ZAF procedure. The results of the electron microprobe analyses are presented in Tables 3–6.

5. Geochemistry

5.1. Whole rock geochemistry

The major and trace element content of the ultramafic to mafic cumulates are presented in Tables 1 and 2. Loss-on-ignition (LOI) values range from 3.5 wt.% to 7 wt.% for the ultramafic cumulates and from 0.8 wt.% to 1.7 wt.% for the mafic cumulates. The wide range of LOI values measured in the ultramafic cumulates indicates a variable serpentinization process, that was most likely controlled by olivine and to lesser extent by pyroxene. The cumulate rocks in the GKO range from highly magnesian (23–34 wt.% MgO) in wehrlite and plagioclase wehrlite, to low magnesian (4–10 wt.% MgO) in the more evolved rocks such as gabbro. The latter show high CaO (11–16 wt.%) and Al_2O_3 (16–25 wt.%). This general trend is consistent with the progressive removal of cumulate phases from the magma.

Selected data on major and trace element content of the GKO cumulate rocks are plotted against MgO in Fig. 8a–h. CaO ranges from 3.65 wt.% to 10.73 wt.% in the ultramafic and from 11 wt.% to 16.33 wt.% in the mafic cumulates (Fig. 8b). Al_2O_3 (Fig. 8a) shows same geochemistry as CaO, with low values in the ultramafic (4.64–10.05 wt.%), and higher amount in the mafic cumulates (15.72–24.78 wt.%). CaO and Al_2O_3 correlate negatively with MgO (Fig. 8a, b), suggesting the accumulation of Ca-rich plagioclase ($An_{87–68}$) in the magma chamber (Fig. 8). The decrease of Ni, Cr and Co content, from higher values in the ultramafic (557–1107 ppm Ni, 195–3269 ppm Cr, and 91–138 ppm Co) to lower values (41–245 ppm Ni, 214–1125 ppm Cr, and 16–42 ppm Co) in the mafic cumulate rocks, is consistent with the fractionation of olivine, spinel and clinopyroxene respectively (Fig. 8c, d). The Ga content varies from 6 ppm to 11 ppm in the ultramafic and from 13 ppm to 18 ppm in the mafic cumulate rocks (Fig. 8e). It correlates negatively with MgO (Fig. 8). The Sr content varies from 16 ppm to 54 ppm in the ultramafic, and from 85 ppm to 191 ppm in the mafic cumulate rocks and increases markedly with decreasing MgO (Fig. 8f) most likely due to higher amount of plagioclase in the mafic cumulates (Grove and Baker, 1984; Beard, 1986; Bağcı et al., 2005, 2006). The variation of the Sc content, from 16 ppm to 105 ppm in the ultramafics and from 25 ppm to 57 ppm in the mafic cumulates (Fig. 8g), correlates with the fractionation of olivine and clinopyroxene (Ross et al., 1954; Borisenko, 1967; Ballantyne, 1992). Vanadium (Fig. 8h), probably included in clinopyroxene (Ross et al., 1954; Borisenko, 1967; Ballantyne, 1992), shows also large variation in both ultramafic (41–132 ppm) and gabbro (39–240 ppm). The incompatible trace elements (Zr, Ba, Rb, Nb, Y etc.) generally show moderate to low concentration (Tables 1 and 2), which reflect their differential partitioning in the cumulus-phase in the magma chamber.

The major element compositions of the ultramafic-mafic cumulates and the isotropic gabbro from the GKO (data from Parlak et al., 2004) are plotted in the AFM diagram (Fig. 9) together with the volcanic arc trend (Brown, 1982), and the fields of the cumulate and the non-cumulate rocks (Beard, 1986). The GKO ultramafic cumulates display a Mg-enrichment whereas the mafic cumulates are enriched in Fe. Both the ultramafic and the mafic cumulate rocks plot in the arc cumulate field of Beard (1986). The isotropic gabbros can be quite well correlated with the volcanic arc trend.

5.2. Mineral chemistry

5.2.1. Olivine

Representative EMP analyses of olivines from the ultramafic and mafic cumulate rocks are presented in Table 3. Olivine crystals are generally homogeneous in composition. The Fo content ranges from 79 mol% to 82 mol% in wehrlites, from 77 mol% to 81 mol% in plagioclase wehrlite, and from 82 mol% to 83 mol% in olivine gabbro. The NiO content slightly decreases from wehrlite (0.14–0.27 wt.%) to olivine gabbro (0.15–0.2 wt.%) in olivine gabbro. Olivine is a good indicator for the relative degree of fractional crystallization as shown for example by the positive correlation between NiO and the forsterite (Fo) contents throughout the cumulates (Fig. 10). The highly magnesian olivines from the ultramafic to mafic cumulate rocks of the GKO differ from olivines that form from a MORB-type melt (Hébert, 1982, 1985). The GKO olivine composition is similar to that from the Mersin (Parlak et al., 1996), Pozantı-Karsantı (Parlak et al., 2000, 2002), Troodos (Hébert and Laurent, 1990), Kızıldağ (Hatay) (Bağcı et al., 2005), Tekirova

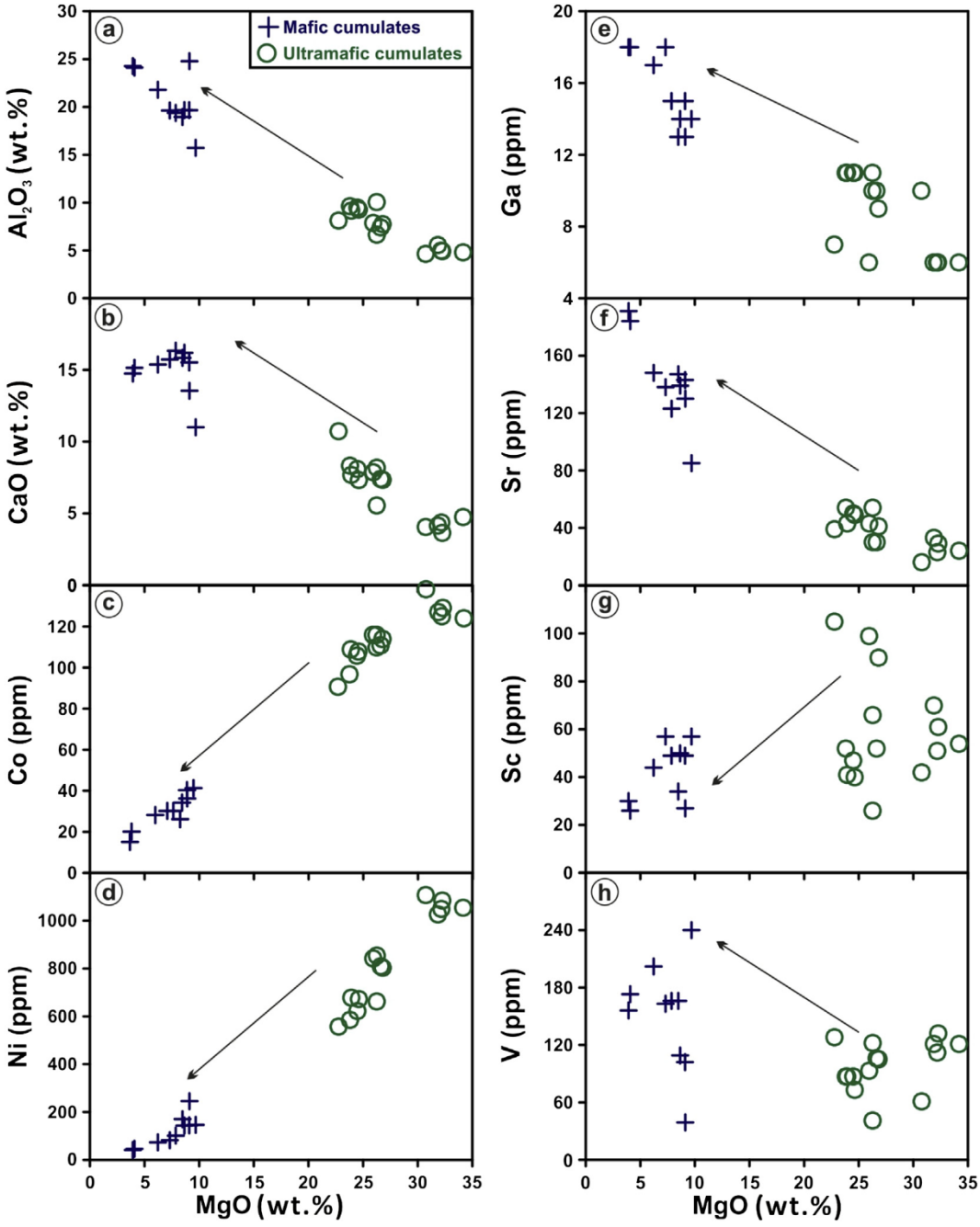

Figure 8. Selected major and trace elements variation diagrams for the cumulate rocks of the Göksun (Kahramanmaraş) ophiolite.

(Antalya) (Bağcı et al., 2006), Kömürhan (Elazığ) (Rızaoğlu et al., 2006) and İspendere (Malatya) (Parlak et al., 2013b) ophiolites, as well as the Tonsina Complex (DeBari and Coleman, 1989), the Border Ranges ultramafic and mafic (BRUM) Complex (Burns, 1985) and the Bay of Island ophiolite (Elthon et al., 1984), which were thought to have formed in a subduction-related tectonic setting.

5.2.2. Clinopyroxene

Table 4 displays selected EMP analyses of clinopyroxenes from the GKO ultramafic and mafic cumulates. The compositions of the clinopyroxenes are shown in Fig. 11. The Fig. 11 shows that cpx from GKO mafic cumulates plots in the field of island arc gabbroic rocks of Burns (1985), whereas those from ultramafic cumulates show a larger spreading, however still within the island arc gabbroic rocks. In terms of quadrilateral end member, the clinopyroxene composition is $En_{44.6–50.28}Fs_{5.33–11.16}Wo_{39.4–49.29}$ in wehrlite, $En_{44.2–55.61}Fs_{6.18–10.72}Wo_{33.67–47.34}$ in plagioclase wehrlite, $En_{49.79–45.73}Fs_{8.97–6.3}Wo_{46.5–41.24}$ in olivine gabbro and $En_{51.39–36.92}Fs_{19.9–8.68}Wo_{47.38–28.7}$ in gabbro (Fig. 11). The Mg# (=100 × Mg/(Mg + Fe)) of clinopyroxene ranges from 82 to 90 in wehrlite, from 82 to 89 in plagioclase wehrlite, from 85 to 89 in olivine gabbro, and from 67 to 85 in gabbro (Table 4). High Mg# of clinopyroxenes from various ophiolitic cumulates and island arcs were documented by many authors (e.g., Elthon et al., 1982, 1984; Komor et al., 1985;

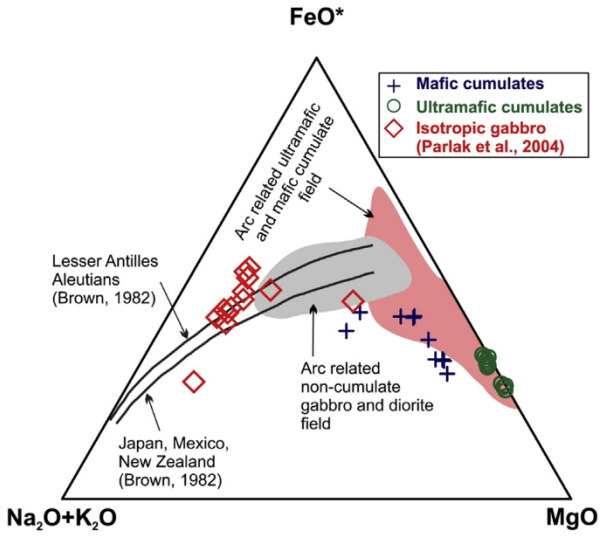

Figure 9. AFM discrimination ternary diagram for the GKO cumulate rocks. Fields of cumulate (pink) and non-cumulate rocks (grey) are from Beard (1986), isotropic gabbro data are from Parlak et al. (2004) and the volcanic arc trend from Brown (1982).

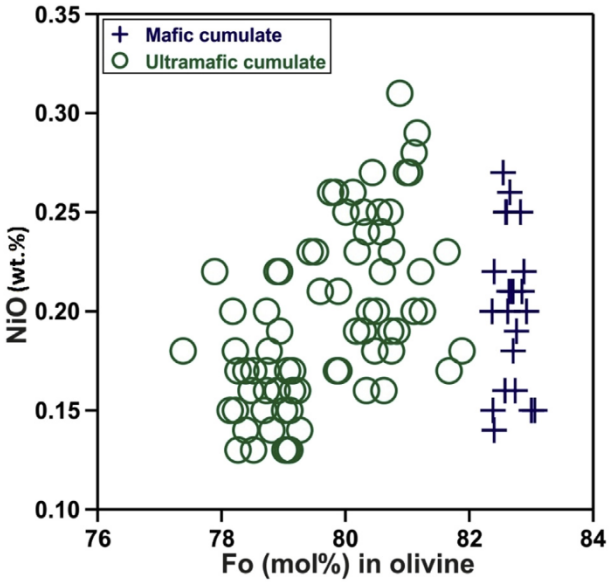

Figure 10. NiO *vs.* Fo in olivines from the cumulate rocks.

DeBari and Coleman, 1989; Parlak et al., 1996, 2000, 2002, 2013b; Bağcı et al., 2005, 2006; Rızaoğlu et al., 2006; Allahyari et al., 2014).

The Cr_2O_3 content is a useful parameter for tracing changes in clinopyroxene compositions during the magmatic differentiation. In the GKO clinopyroxene, it ranges from 0 to 1.1 wt.% in the ultramafic cumulates and from 0.19 wt.% to 1.4 wt.% in olivine gabbro, and up to 0.6 wt.% in gabbro (Table 4). The Cr_2O_3 content in the cumulate rocks shows a slight decrease with decreasing Mg# from ultramafic to mafic cumulates (Fig. 12a), which may be related to a gradual Cr depletion of the magma during differentiation (Hodges and Papike, 1976). The GKO clinopyroxenes plot in the (experimental) field of low-pressure of N-type MORB (Elthon, 1987). Clinopyroxenes in cumulates are characterized by low TiO_2 content, with an average of 0.52 wt.%, which shows generally negative correlation with Mg# (Table 4). The TiO_2 content of clinopyroxenes in mantle tectonites from other areas in Turkey (Köyceğiz (Muğla): 0.07–0.32 wt.%; Orhaneli (Bursa): 0.11 wt.%; Refahiye (Erzincan): 0.16–0.41 wt.%) is also low (Uysal et al., 2012, 2015, 2017). According to Pearce and Norry (1979), the amount of Ti in clinopyroxene reflects the degree of depletion of the mantle source, as well as the Ti activity of the parental magma that generated the cumulates. The very low Ti content in clinopyroxene from both tectonites and cumulates suggests that one or several earlier partial melting events removed Ti from the mantle clinopyroxenes (Duncan and Green, 1980; Hébert and Laurent, 1990). Thus, the crystallization of GKO clinopyroxenes from a Ti-poor magma seems plausible. Elthon (1987) suggested that clinopyroxene, formed at moderate or higher pressure, also have high Al_2O_3 (>3 wt.%) and TiO_2 (>1 wt.%) content. The Al_2O_3 and TiO_2 content of clinopyroxenes from the GKO cumulate rocks are plotted in Fig. 12b. Low- and moderate-pressure clinopyroxenes from the gabbroic rocks of the Mid-Cayman Rise spreading center are also plotted for comparison. The data from the cumulate rocks plot within the field of low-pressure clinopyroxenes from the Semail ophiolite and mid-pressure clinopyroxenes of the Mid-Cayman Rise (Fig. 12b). The experimental data on clinopyroxene suggests that the increase of Al_2O_3 may be due to higher temperature or pressure (Herzberg, 1978). The Al_2O_3 content clinopyroxene from the ultramafic and mafic cumulates is constant and does not vary with increasing Mg# (Fig. 12c). The variation of Al_2O_3 *vs.* Mg# is perpendicular to the trend of a typical high-pressure field defined by Medaris (1972), but parallel to the trend of typical low-pressure cumulates such as the Semail ophiolite, Pozantı-Karsantı ophiolite, Skaergaard intrusion and the high-level gabbros from the Tonsina Complex (DeBari and Coleman, 1989). All these evidences suggest that the GKO cumulates were formed in low-pressure conditions, representative for the shallow levels of an island arc.

The plot of clinopyroxenes from the GKO cumulates into the SiO_2 *vs.* Al_2O_3 discrimination diagram of Le Bas (1962) and Ti *vs.* Ca + Na diagram of Leterrier et al. (1982) demonstrates their origin from a subalkaline source (Fig. 13a,b). Al and Ti contents of clinopyroxenes help to discriminate between the mid-ocean ridge (MOR) and the island arc settings (Beccaluva et al., 1989). Fig. 14 displays the low-Al and Ti, content in the clinopyroxenes of the mafic cumulate rocks from the GKO and their plot in the island arc tholeiite field.

5.2.3. *Plagioclase*

Representative analyses of plagioclases from the ultramafic and mafic cumulates are presented in Table 5. Plagioclases contain 45.5–51.6 wt.% SiO_2, 30.7–34.20 wt.% Al_2O_3, 13.5–18.5 wt.% CaO, 1.24–3.9 wt.% Na_2O and 0–0.07 wt.% K_2O. The compositional range

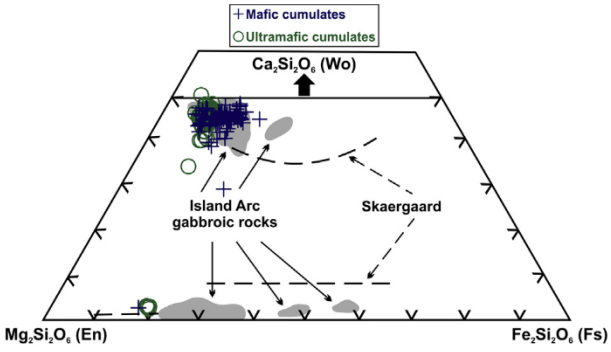

Figure 11. Plot of the composition of clinopyroxene and orthopyroxene from the GKO mafic and ultramafic cumulate rocks in the ternary diagram of Morimoto et al. (1988). Fields of island arc gabbroic rocks and Skaergaard trends are from Burns (1985).

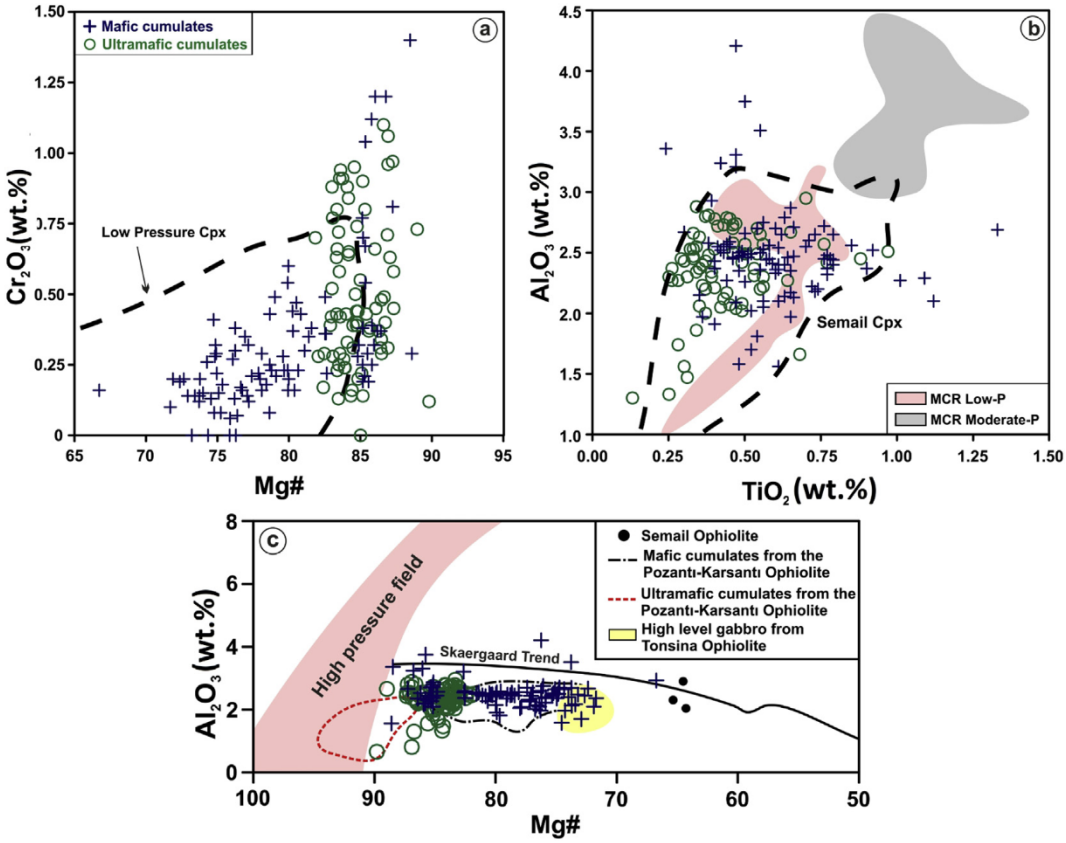

Figure 12. (a) Cr_2O_3 vs. Mg# in clinopyroxenes from the GKO cumulate rocks. Low-pressure cpx field is from 1-atm experimental studies of N-MORB (Elthon, 1987). (b) Al_2O_3 vs. TiO_2 content from clinopyroxenes in the cumulate rocks. Fields of the Mid-Cayman Rise (MCR) low-pressure and moderate-pressure gabbroic rocks are from Elthon (1987). Semail ophiolite data (dashed bold line) are from Pallister and Hopson (1981). (c) Al_2O_3 vs. Mg# in the clinopyroxenes from the cumulate rocks. The field of high-pressure peridotite is from Medaris (1972). Fields of ultramafic and mafic cumulates are from Parlak et al. (2000, 2002).

is narrow for plagioclases from the ultramafic cumulates (An_{84-89}) and olivine gabbro (An_{81-87}). In contrast, plagioclase from gabbros shows zoning, with a Ca-rich core ($\sim An_{84}$) and a rim enriched in Na ($\sim An_{66}$), indicating instable chemical equilibrium within the magma chamber. The high An content of plagioclase in the ultramafic to mafic cumulates is similar to that found in suprasubduction-zone-type ophiolites in the eastern Mediterranean (Hébert and Laurent, 1990; Parlak et al., 1996, 1997, 2000, 2013b; Bağcı et al., 2005, 2006; Rızaoğlu et al., 2006) and in the arc-related igneous rocks (Arculus and Wills, 1980; Dupuy et al., 1982; Beard, 1986; Fujimaki, 1986; DeBari et al., 1987; DeBari and Coleman, 1989). The high-An plagioclase is due to high water (Arculus and Wills, 1980; Sisson and Grove, 1993; Panjasawatwong et al., 1995) and high Ca/(Ca + Na) melt contents (Panjasawatwong et al., 1995). Plagioclases from the ultramafic and mafic cumulates of the GKO are likely to have been derived from a liquid with a high CaO/Na_2O ratio and/or, which crystallized under high H_2O content.

5.2.4. Orthopyroxene

Selected analyses of orthopyroxene from the ultramafic and mafic cumulates are presented in Table 6. They have a mostly enstatitic composition and contain 54.7–55.1 wt.% SiO_2, 0.38–0.65 wt.% TiO_2, 1.26–1.55 wt.% Al_2O_3, 29.2–30.2 wt.% MgO, 1.31–1.63 wt.% CaO, 0.26–0.33 wt.% MnO. The composition of orthopyroxene is shown also in Fig. 11. In terms of quadrilateral components, orthopyroxene compositions are $En_{79}Fs_{18}Wo_3$ in wehrlite, $En_{78-79}Fs_{18-19}Wo_{2.5-3}$ in plagioclase wehrlite and $En_{81}Fs_{17}Wo_3$ in olivine gabbro. The composition of GKO orthopyroxene is consistent with the composition of orthopyroxene from the gabbroic rocks formed in an island arc setting (DeBari and Coleman, 1989; Parlak et al., 1996, 2000) (Fig. 11).

6. Discussion

6.1. Petrogenesis

Whole rock and mineral compositions of the mafic-ultramafic cumulates provide solid constraints for understanding the petrogenetic processes of these rocks. As an example, plagioclases, clinopyroxenes and olivines from gabbroic rocks can be used. Their compositions differ among those, which were generated in mid-ocean ridge, back-arc basin, or stratiform complexes (Burns, 1985). Fig. 15a presents the covariation of anorthite content in plagioclase *vs.* Mg# in clinopyroxene from the gabbroic cumulates of the GKO, compared with the fields of suprasubduction zone type (SSZ-type) ophiolites in Turkey (Parlak et al., 1996, 2000, 2013b; Bağcı et al., 2005, 2006; Rızaoğlu et al., 2006). The GKO gabbroic cumulate rocks display a transitional trend between the fields of MORB gabbro and arc gabbro. Some of the samples overlap to the field of arc-related gabbro and differ from the gabbroic rocks formed in a mid-ocean ridge setting in terms of their high anorthite content of plagioclase (Fig. 15a). The variation of An content in plagioclase *vs.* Mg# in olivine for the GKO gabbroic rocks are presented in Fig. 15b together with some eastern Mediterranean ophiolites and other well-documented arc settings. The mineral composition of the gabbroic rocks in the

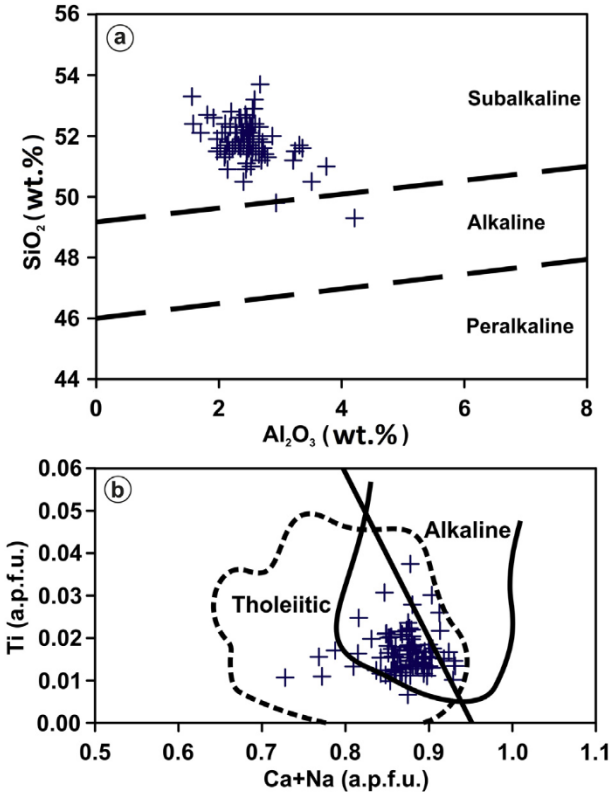

Figure 13. Discrimination diagrams for clinopyroxenes of the gabbroic cumulates: (a) SiO_2 *vs.* Al_2O_3 plot (diagram of Le Bas, 1962), (b) plot of Ti (a.p.f.u. = atoms per formula unit) *vs.* Ca + Na (diagram of Leterrier et al., 1982).

GKO differ from the composition of the MORB cumulates (Hébert and Laurent, 1990), showing high fractionation trends in terms of $An_{50–90}$ and $Fo_{65–90}$ contents. They exhibit a close similarity to suprasubduction-zone-type ophiolites from the eastern Mediterranean region and several known island arc settings (Fig. 15b). The experimental studies demonstrated that the increase of the pressure under anhydrous conditions results in a decrease of the An content in plagioclase coexisting with olivine (Green, 1969; Bender et al., 1978). In contrast, the effect of H_2O activity on the equilibrium of plagioclase composition increases the An content (Yoder, 1969; Johannes, 1978; Takagi et al., 2005; Hamada and Fujii, 2007). Consequently, the crystallization of the high-An plagioclases in the gabbroic rocks from island arcs (Jaques, 1981; Dupuy et al., 1982; Beard, 1986; Fujimaki, 1986; DeBari et al., 1987; DeBari and Coleman, 1989; Thy et al., 1989) has been attributed to the presence of H_2O in the melt during crystallization (Helz, 1973). In this respect, our results suggest that the formation of the gabbroic cumulates of the GKO took place above an intraoceanic subduction.

6.2. Modern analogues

The GKO displays a complete oceanic lithospheric section, namely mantle tectonites, ultramafic to mafic cumulates, isotropic gabbros, sheeted dykes with plagiogranite and basic to acidic volcanic-sedimentary rock association (Parlak et al., 2004). The GKO volcanics, the sheeted dykes and the isotropic gabbros chemistry suggest that they have formed in a subduction-related tectonic setting (Parlak et al., 2004). The wide-spread volcano-sedimentary unit is interpreted as an ensimatic island arc assemblage, built on a SSZ-type crust in Late Cretaceous (Parlak et al., 2004; Rızaoğlu et al., 2006; Robertson et al., 2007).

Modern analogues of the Late Cretaceous SSZ-type ophiolites in Turkey are found in forearc areas of the SW Pacific region. Widespread arc-related tholeiitic volcanics and boninites have been reported from the Eocene Izu–Bonin–Mariana arc (Bloomer and Hawkins, 1983; Pearce et al., 1992; Stern and Bloomer, 1992; Taylor, 1992), the Tonga arc and Cape Vogel in Papua New Guinea (Hawkins, 1995). In addition, deeper-level oceanic crust (gabbro, dolerite and serpentinized harzburgites) have been dredged from the Tonga trench (Sharaskin et al., 1983; Falloon et al., 1987). Reagan et al. (2010) stated that the geochemical similarity between the forearc basalts (FAB) to boninite sequence in the Izu-Bonin-Mariana (IBM) island on one side, and the shallow crustal sections of many ophiolites on the other side, indicates that these ophiolites represent an obducted forearc lithosphere generated during subduction initiation rather than a backarc or mid-ocean ridge type oceanic lithosphere. The similarity between the Mariana forearc stratigraphy and that found in Cretaceous and Jurassic Tethyan ophiolites suggests that these ophiolites were associated with the initiation of the subduction that closed the Tethys Ocean and affected the movement of the adjacent plates (Reagan et al., 2010).

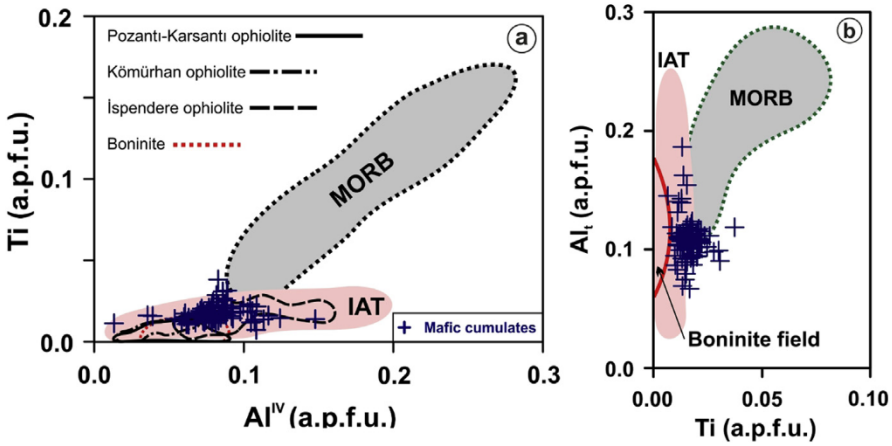

Figure 14. Tectonic classification diagrams for clinopyroxenes from the GKO gabbroic cumulates: (a) Ti *vs.* Al^{IV} plot (after Beccaluva et al., 1989). Fields of the Pozantı-Karsantı, Kömürhan and İspendere ophiolites are from Parlak et al. (2002) and Rızaoğlu et al. (2006). (b) Al_t *vs.* Ti plot (diagram of Beccaluva et al., 1989).

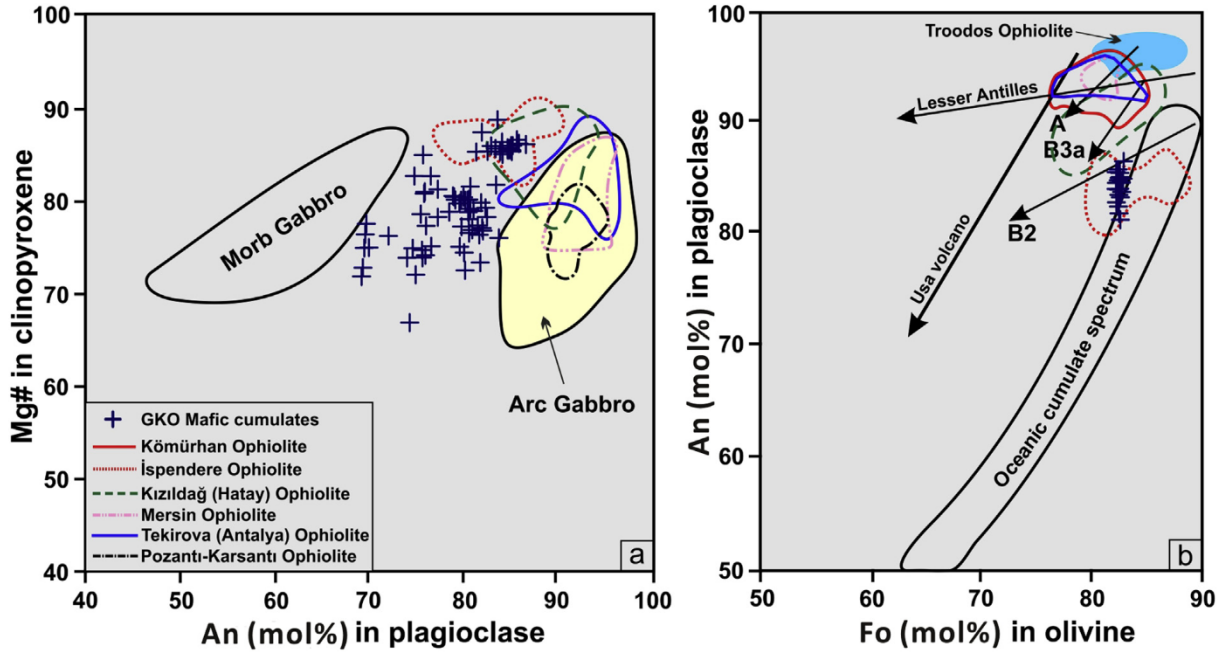

Figure 15. (a) Composition of coexisting plagioclase (An in mol%) and clinopyroxene (Mg#) in the GKO gabbroic cumulates, compared to the MORB and arc gabbro (Burns, 1985), the Mersin cumulates and the Pozantı-Karsantı, Kızıldağ and Tekirova ophiolites (data from Parlak et al., 1996, 2000 and Bağcı et al., 2005, 2006), the İspendere (Parlak et al., 2013b) and the Kömürhan ophiolites (Rızaoğlu et al., 2006). (b) Anorthite content in plagioclase (mol%) *vs.* Fo (mol%) content in olivine for the mafic cumulates, compared with the Troodos (Hébert and Laurent, 1990), Mersin and İspendere (Parlak et al., 1996, 2013b), the Kızıldağ and Tekirova (Bağcı et al., 2005, 2006), the Kömürhan (Rızaoğlu et al., 2006) ophiolites. The B2 and B3a— the Boisa volcano (Gust and Johnson, 1981), the Usa volcano after Fujimaki (1986); A—the Agrigan volcano (Stern, 1979) and Lesser Antilles after Arculus and Wills (1980).

6.3. *Paleogeography and geodynamic setting*

The southeast Anatolian orogeny exposes ophiolites sequence with well-preserved oceanic lithospheric sections that support a better understanding of the tectonic setting, timing of genesis and the emplacement of the ophiolites. In southeast Turkey, there are two ophiolite belts, located to the south and north of the Bitlis-Pütürge continental sliver (Robertson et al., 2007; Parlak et al., 2009, 2013b). The northern belt occurs between the Tauride platform and the Bitlis-Pütürge massif and includes, from west to east, the Göksun (Kahramanmaraş) ophiolite, the Berit meta-ophiolite, the İspendere (Malatya) ophiolite, the Kömürhan ophiolite and the Guleman (Elazığ) ophiolite (Yazgan and Chessex, 1991; Genç et al., 1993; Parlak et al., 2004, 2009; Rızaoğlu et al., 2006; Robertson et al., 2007) (Fig. 16a). The northern belt ophiolites exhibit geochemical evidence of being formed by spreading above an intra-oceanic subduction zone within the Berit Ocean (Parlak et al., 2009; Robertson et al., 2012, 2013b) (Fig. 16b). The ophiolites were then accreted beneath the Tauride active continental margin during the Late Cretaceous. The ophiolites and the over-riding platform are cut by Late Cretaceous to Eocene calc-alkaline granitic rocks (Yazgan and Chessex, 1991; Rızaoğlu et al., 2009; Karaoğlan et al., 2013b, 2016). The arc magmatism has been attributed to the northward subduction of the oceanic crust along an Andean-type continental margin (Robertson, 2002; Parlak et al., 2006; Robertson et al., 2006, 2007; Parlak et al., 2009; Rızaoğlu et al., 2009; Karaoğlan et al., 2013b, 2016). The southern ophiolites belt occurs between the Bitlis-Pütürge massif and the Arabian platform and includes the Kızıldağ (Hatay) and Koçali (Adıyaman) ophiolites in Turkey, and the Baer-Bassit ophiolite in Syria, the latter contiguous with the Troodos ophiolite to the west (Robertson et al., 2012, 2013) (Fig. 16a). These ophiolites are also inferred to be formed in a SSZ setting, developed above a northward-dipping intraoceanic subduction zone (Al-Riyami et al., 2002; Bağcı et al., 2005, 2008; Rızaoğlu et al., 2006; Parlak et al., 2009, 2013b). The southern belt ophiolites were emplaced southwards onto the Arabian continental margin during Campanian–Maastrichtian time (Robertson, 1986a, b; Tekeli and Erendil, 1986).

A number of differences between the northern and southern belt ophiolites can be presented in terms of petrology, geochronology and field relations. The northern belt ophiolites are characterized by: (i) containing more evolved crustal rocks (Parlak et al., 2004; Rızaoğlu et al., 2006); (ii) a lava unit is intercalated within the pelagic carbonates (Rızaoğlu et al., 2006; Robertson et al., 2007); (iii) except the Guleman ophiolite, they are, together with the Malatya-Keban platform, intruded by Late Cretaceous–Eocene granitoids (Parlak et al., 2006; Rızaoğlu et al., 2009; Kuşçu et al., 2010; Karaoğlan et al., 2013b, 2016); (iv) they are tectonically overlain by the Tauride platform and, in turn, they tectonically overlie the Middle Eocene Maden Group/Complex (Parlak et al., 2004; Robertson et al., 2006, 2007); this indicates a Late Cretaceous and Eocene tectonic emplacement; and (v) zircon U-Pb age of gabbros from the Göksun, İspendere and Kömürhan ophiolites ranges from 88 Ma to 84 Ma (Karaoğlan et al., 2012).

In contrast, the southern belt ophiolites are characterized by: (i) the prevalence of basic to highly depleted boninite-type plutonics and extrusives, suggesting a forearc setting (Al-Riyami et al., 2002; Bağcı et al., 2005, 2008); (ii) volcanics locally interbedded with, or overlain by metalliferous oxide sediments (Robertson, 1986b); (iii) southwards emplacement onto the Arabian continental margin during Campanian–Maastrichtian time (Tekeli and Erendil, 1986); (iv) lack of granitic intrusion; (v) lack of Eocene contractional tectonics affecting the Arabian platform; and (vi) an age of ~92 Ma for

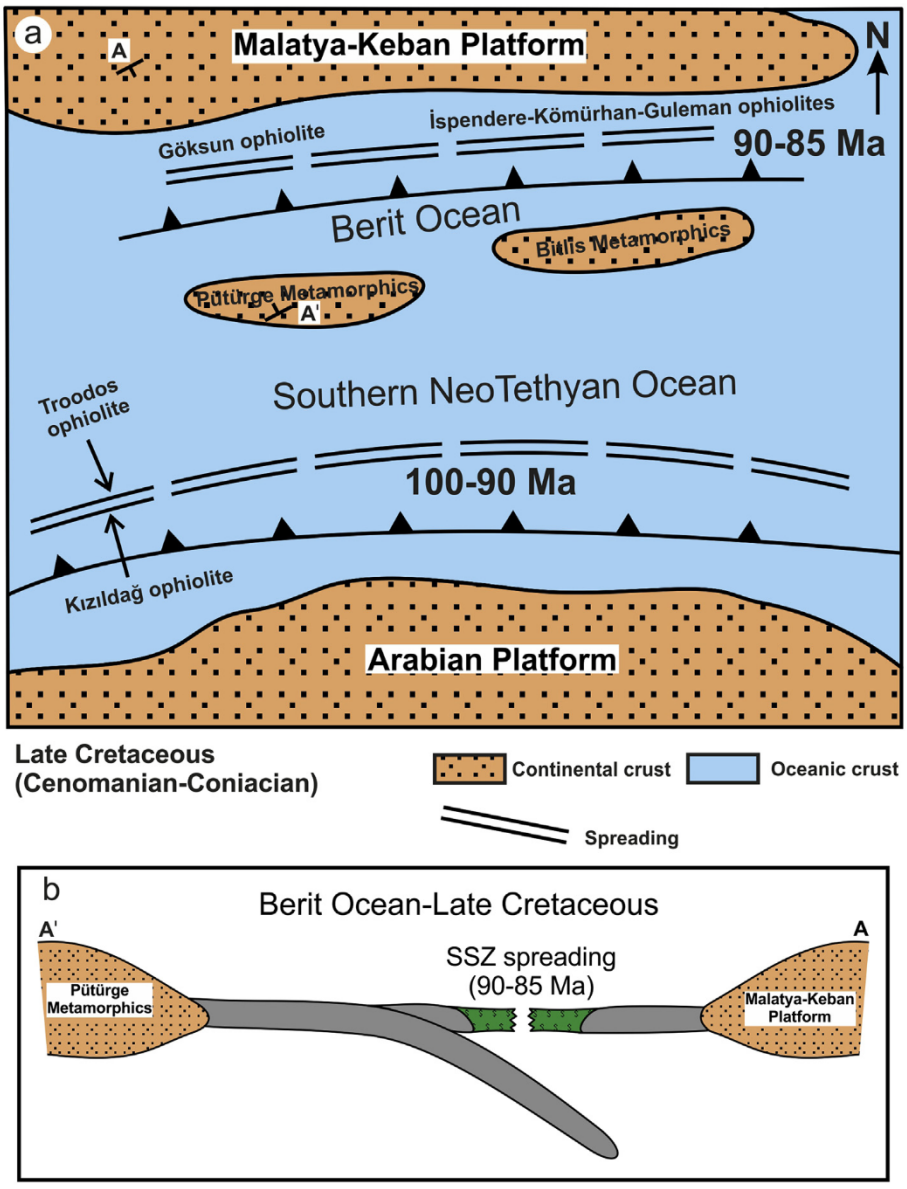

Figure 16. (a) Reconstruction of the Late Cretaceous paleogeography with the Southern Neotethys and the related southerly oceanic strands (after Karaoğlan et al., 2012; Robertson et al., 2012). (b) Geodynamic setting of the Göksun ophiolite within the Berit Ocean between the Malatya-Keban platform and Pütürge metamorphics. Cross-section line is indicated in Fig. 16a.

the Hatay and the Troodos ophiolites (Mukasa and Ludden, 1987; Dilek and Thy, 2009; Karaoğlan et al., 2013a). In addition, the Bitlis and the Pütürge metamorphic units of the southern Turkey were affected by HP-LT and LP-LT metamorphism, both during the uppermost Cretaceous (Oberhänsli et al., 2010). This indicates that rifted continental blocks subducted and then exhumed at 74 Ma during the closure of the southern Neotethys. All the evidence supports the existence of two separate SSZ-spreading centres in the southern Neotethys, one to the north and one to the south of the Bitlis-Pütürge massif.

7. Conclusions

(1) All the evidence supports the assumption that the GKO formed in Late Cretaceous above a north-dipping intraoceanic subduction zone between the Taurides to the north and the Bitlis-Pütürge massif to the south, within the Berit Ocean.

(2) The major and trace element geochemistry as well as the mineral chemistry of the ultramafic to mafic cumulate rocks suggest that the primary magma generating the GKO was compositionally similar to that observed in modern island-arc tholeiitic environment.

(3) The geochemical data between the upper (volcanics, sheeted dykes and isotropic gabbro) (Parlak et al., 2004) and the lower (ultramafic to mafic cumulates) crustal rocks in the GKO were derived from a similar magma source, suggesting that they were genetically related.

(4) The mineral chemistry of the ultramafic to mafic cumulates indicates that they were derived from a mantle source that was previously depleted by earlier partial melting events, causing crystallization of clinopyroxenes from a Ti-poor magma.

(5) The crystallization order for the cumulate rocks is: olivine ± chromian spinel → clinopyroxene → plagioclase. The highly magnesian olivine (Fo_{77-83}) and clinopyroxene (Mg# of

82–90) and highly Ca-plagioclase ($An_{81–89}$) show a close similarity to the eastern Mediterranean ophiolites that formed in a supra-subduction zone (SSZ) setting during the closure of several Neotethyan oceanic basins.

(6) The field and the geochemical evidence suggest that the GKO were only a part of a much larger sheet of oceanic lithosphere that accreted to the base of the Tauride active continental margin contemporaneously and genetically/tectonically related to the İspendere, Kömürhan and the Guleman ophiolites.

Acknowledgment

Emilio Saccani, Laura Gaggero and anonymous reviewer are thanked for their constructive and very valuable comments that improved the quality of the paper. The authors would like to thank Fabio Capponi for performing XRF major and trace element analyses at Geneva (Switzerland) University. Dan Topa is thanked for his guidance during the microprobe analysis at Salzburg (Austria) University. This research was supported by TÜBİTAK (YDABÇAG-199Y011) and the Çukurova University Scientific Research Projects (MMF2002BAP41). OP acknowledges the Open Fund (GPMR201702) of State Key Lab of Geological Processes and Mineral Resources, China University of Geosciences, Wuhan. CI acknowledges subsidy by the Russian Government to support the Program of competitive growth of Kazan Federal University.

Appendix A. Supplementary data

Supplementary data to this article can be found online at https://doi.org/10.1016/j.gsf.2018.11.004.

References

Aktaş, G., Robertson, A.H.F., 1984. The Maden complex, SE Turkey: evolution of a Neotethyan continental margin. In: Dixon, J.E., Robertson, A.H.F. (Eds.), The Geological Evolution of the Eastern Mediterranean, vol. 17. Geological Society, London, Special Publication, pp. 375–402.

Allahyari, K., Saccani, E., Rahimzadeh, B., Zeda, O., 2014. Mineral chemistry and petrology of highly magnesian ultramafic cumulates from the Sarve-Abad (Sawlava) ophiolites (Kurdistan, NW Iran): new evidence for boninitic magmatism in intra-oceanic forearc setting in the Neo-Tethys between Arabia and Iran. Journal of Asian Earth Sciences 79, 312–328.

Al-Riyami, K., Robertson, A.H.F., Dixon, J., Xenophontos, C., 2002. Origin and emplacement of the Late Cretaceous Baer-Bassit ophiolite and its metamorphic sole in NW Syria. Lithos 65, 225–260.

Arculus, R.J., Wills, K.J.A., 1980. The petrology of plutonic blocks and inclusions from Lesser Antilles island arc. Journal of Petrology 21, 743–799.

Bağcı, U., Parlak, O., Höck, V., 2005. Whole rock and mineral chemistry of cumulates from the Kızıldağ (Hatay) ophiolite (Turkey): clues for multiple magma generation during crustal accretion in the southern Neotethyan ocean. Mineralogical Magazine 69, 39–62.

Bağcı, U., Parlak, O., Höck, V., 2006. Geochemical character and tectonic environment of ultramafic to mafic cumulates from the Tekirova (Antalya) ophiolite (southern Turkey). Geological Journal 41, 193–219.

Bağcı, U., Parlak, O., Höck, V., 2008. Geochemistry and tectonic environment of diverse magma generations forming the crustal units of the Kızıldağ (Hatay) ophiolite southern Turkey. Turkish Journal of Earth Sciences 17, 43–71.

Ballantyne, P., 1992. Petrology and geochemistry of the plutonic rocks of the Halmahera ophiolite, eastern Indonesia, an analogue of modern oceanic forearcs. In: Parson, L.M., Murton, B.J., Browning, P. (Eds.), Ophiolites and Their Modern Oceanic Analogues, vol. 60. Geological Society, London, Special Publication, pp. 179–202.

Baştuğ, M.C., 1980. Sedimentation, deformation and melange emplacement in Lice Basin, Dicle-karabegan Area, South East Turkey. Ph.D thesis. Middle East Technical University, p. 282.

Beard, J.S., 1986. Characteristic mineralogy of arc-related cumulate gabbros: implications for the tectonic setting of gabbroic plutons and for andesite genesis. Geology 14, 848–851.

Beccaluva, L., Macciotta, G., Piccardo, G.B., Zeda, O., 1989. Clinopyroxene composition of ophiolite basalts as petrogenetic indicator. Chemical Geology 77, 165–182.

Bender, J.F., Hodges, F.N., Bence, A.E., 1978. Petrogenesis of basalts from the project FAMOUS area: experimental study from 0 to 15 kbar. Earth and Planetary Science Letters 41, 277–302.

Bloomer, S.H., Hawkins, J.W., 1983. Gabbroic and ultramafic rocks from the Mariana trench: an island arc ophiolite. In: Hayes, D.E. (Ed.), The Tectonic and Geologic Evolution of Southeast Asian Seas. 2nd American Geophysical Union, Washington, D.C., pp. 294–317

Borisenko, L.F., 1967. Trace elements in pyroxenes and amphiboles from ultramafic rocks of the Urals. Mineralogical Magazine 36, 403–410.

Burns, L.E., 1985. The Border Ranges ultramafic and mafic complex, south central Alaska: cumulate fractionates of island arc volcanics. Canadian Journal of Earth Sciences 22, 1020–1038.

Brown, G.C., 1982. Calc-alkaline intrusive rocks: their diversity, evolution and relation to volcanic rocks. In: Thorpe, R.S. (Ed.), Andesites: orogenic andesites and related rocks. Wiley, New York, pp. 437–461.

Çelik, O.F., Marzoli, A., Marschik, R., Chiaradia, M., 2011. Early-Middle Jurassic intra-oceanic subduction in the İzmir-Ankara-Erzincan ocean, northern Turkey. Tectonophysics 509, 120–134. https://doi.org/10.1016/j.tecto.2011.06.007.

DeBari, S., Kay, S.M., Kay, R.W., 1987. Ultramafic xenoliths from Adagdak volcano, Adak, Aleutian islands, Alaska: deformed igneous cumulates from the Moho of an island arc. Journal of Geology 95, 329–341.

DeBari, S.M., Coleman, R.G., 1989. Examination of the deep levels of an island arc: evidence from the Tonsina ultramafic-mafic assemblage, Tonsina, Alaska. Journal of Geophysical Research 94, 4373–4391.

Deer, W.A., Howie, R.A., Zussman, J., 1992. An Introduction to the Rock-forming Minerals, second ed. Pearson Prentice Hall, London, p. 696.

Dewey, J.F., Hempton, M.R., Kidd, W.S.F., Şaroğlu, F., Şengör, A.M.C., 1986. Shortening of continental lithosphere; the neotectonics of eastern Anatolia, a young collision zone. In: Coward, M.P., Ries, A.C. (Eds.), Collision Tectonics, 19. Geological Society, London, Special Publication, pp. 3–36.

Dilek, Y., Flower, M.F.J., 2003. Arc-trench rollback and forearc accretion: 2. A model template for ophiolites in Albania, Cyprus, and Oman. In: Dilek, Y., Robinson, P.T. (Eds.), Ophiolites in Earth History, vol. 218. Geological Society, London, Special Publication, pp. 43–68.

Dilek, Y., Furnes, H., Shallo, M., 2008. Geochemistry of the Jurassic Mirdita ophiolite (Albania) and the MORB to SSZ evolution of a marginal basin oceanic crust. Lithos 100, 174–209. https://doi.org/10.1016/j.lithos.2007.06.026.

Dilek, Y., Thy, P., 2006. Age and petrogenesis of plagiogranite intrusions in the Ankara mélange central Turkey. Island Arc 15, 44–57.

Dilek, Y., Thy, P., 2009. Island arc tholeiite to boninitic melt evolution of the Cretaceous Kızıldağ (Turkey) ophiolite: model for multi-stage early arc-forearc magmatism in Tethyan subduction factories. Lithos 113, 68–87.

Duncan, R.A., Green, D.H., 1980. Role of multi-stage melting in the formation of oceanic crust. Geology 8, 22–26.

Dupuy, C., Dostal, J., Marcelot, G., Bougault, H., Joron, J.L., Treuil, M., 1982. Geochemistry of basalt from central and southern New Hebrides arc: implications for their source rock composition. Earth and Planetary Science Letters 60, 207–225.

Elthon, D., 1987. Olivine-liquid partitioning in high-MgO basalt and komatites. In: 18th Lunar and Planetary Science Conference, pp. 258–259. Abstracts.

Elthon, D., Casey, J.F., Komor, S., 1982. Mineral chemistry of ultramafic cumulates from the North Arm Mountain Massif of the Bay of Islands ophiolite: evidence for high-pressure crystal fractionation of oceanic basalts. Journal of Geophysical Research 87 (B10), 8717–8734.

Elthon, D., Casey, J.F., Komor, S., 1984. Cryptic mineral chemistry variations in a detailed traverse through the cumulate ultramafic rocks of the North Arm Mountain massif of the Bay of Island ophiolite, Newfoundland. In: Gass, I.G., Lippard, S.J., Shelton, A.W. (Eds.), Ophiolites and Oceanic Lithosphere. Blackwell, London, pp. 83–97.

Falloon, T.J., Green, D.H., Crawford, A., 1987. Dredged igneous rocks from the northern termination of the Tofua magmatic arc, Tonga and adjacent Lau Basin. Australian Journal of Earth Sciences 34, 487–506. https://doi.org/10.1080/08120098708729428.

Fujimaki, H., 1986. Fractional crystallization of the basaltic suite of USA volcano, southwest Hokkaido, Japan, and its relationships with the associated felsic suite. Lithos 19, 129–140.

Genç, Ş.C., Yiğitbaş, E., Yılmaz, Y., 1993. Geology of the Berit Metaophiolite, A. Suat Erk Jeoloji Sempozyumu, Bildiriler, pp. 37–52.

Green, T.H., 1969. High pressure experimental studies on the origin of anorthosite. Canadian Journal of Earth Sciences 6, 427–440.

Grove, T.L., Baker, M.B., 1984. Phase equilibrium controls on the tholeiitic versus calc-alkaline differentiation trends. Journal of Geophysical Research 89, 3253–3274.

Gust, D.A., Johnson, R.W., 1981. Amphibole bearing cumulates from Boisa Island, Papua New Guinea: evalution of the role of fractional crystallization in an andesitic volcano. Journal of Geology 89, 219–232.

Hamada, M., Fujii, T., 2007. H_2O-rich island arc low-K tholeiite magma inferred from Ca-rich plagioclase-melt inclusion equilibria. Geochemical Journal 41, 437–461.

Hawkins, J.W., 1995. Evolution of the Lau basin: insights from ODP Leg 135. In: Taylor, B., Natland, J. (Eds.), Active Margins and Marginal Basins of the Western Pacific, vol. 88. American Geophysical Union Geophysical Monograph, pp. 125–173.

Hébert, R., 1982. Petrography and mineralogy of oceanic peridotites and gabbros: some comparisons with ophiolite examples. Ofioliti 2 (3), 299–324.

Hébert, R., 1985. Pétrologie des roches ignées océaniques et comparison avec les complexes ophiolitiques du Québec, de Chypre et de l'Apennin. Thèse d'Etat, Université de Bretagne Occidentale, Brest, p. 542 (in French).

Hébert, R., Laurent, R., 1990. Mineral chemistry of the plutonic section of the Troodos ophiolite: new constraints for genesis of arc-related ophiolites. In: Malpas, J., Moores, E., Panayiotou, A., Xenophontos, C. (Eds.), Proceedings of Troodos Ophiolite Symposium, Cyprus, pp. 149–163.

Helz, R.T., 1973. Phase relations of basalt in their melting range at P_{H2O}=5 kb as a function of oxygen fugacity. I. Mafic Phases. Journal of Petrology 14, 249–302.

Herzberg, C.T., 1978. Pyroxene geothermometry and geobarometry: experimental and thermodynamic evaluation of some subsolidus phase relations involving pyroxenes in the system CaO-MgO-Al_2O_3 -SiO_2. Geochimica et Cosmochimica Acta 42, 945–957.

Hodges, F.N., Papike, J.J., 1976. DSDP site 334: magmatic cumulates from ocean layer 3. Journal of Geophysical Research 81, 4135–4151.

Jaques, A.L., 1981. Petrology and petrogenesis of cumulate peridotite and gabbro from the Marum ophiolite complex, northern Papua-New Guinea. Journal of Petrology 22, 1–40.

Johannes, W., 1978. Melting of plagioclase in the system Ab-An-H_2O and Qz-Ab-An-H_2O at P_{H2O}=5 kbars, an equilibrium problem. Contributions to Mineralogy and Petrology 66, 295–303.

Karaoğlan, F., Parlak, O., Hejl, E., Neubauer, F., Klötzli, U., 2016. The temporal evolution of the active margin along the Southeast Anatolian Orogenic Belt (SE Turkey): evidence from U-Pb, Ar-Ar and fission track chronology. Gondwana Research 33, 190–208.

Karaoğlan, F., Parlak, O., Klötzli, U., Thöni, M., Koller, F., 2013a. U-Pb and Sm-Nd geochronology of the Kızıldağ (Hatay, Turkey) ophiolite: implications for the timing and duration of suprasubduction zone type oceanic crust formation in the Southern Neotethys. Geological Magazine 150, 283–299.

Karaoğlan, F., Parlak, O., Klötzli, U., Koller, F., Rızaoğlu, T., 2013b. Age and duration of intra-oceanic arc volcanism built on a suprasubduction zone type oceanic crust in southern Neotethys, SE Anatolia. Geoscience Frontiers 4, 399–408.

Karaoğlan, F., Parlak, O., Robertson, A.H.F., Thöni, M., Klötzli, U., Koller, F., Okay, A.İ., 2013c. Evidence of Eocene high-temperature/high-pressure metamorphism of ophiolitic rocks and granitoid intrusion related to Neotethyan subduction processes (Doğanşehir area, SE Anatolia). In: Robertson, A.H.F., Parlak, O., Ünlügenç, U.C. (Eds.), Geological Development of Anatolia and the Easternmost Mediterranean Region, vol. 372. Geological Society, London, Special Publication, pp. 249–272.

Karaoğlan, F., Parlak, O., Klötzli, U., Thöni, M., Koller, F., 2012. U-Pb and Sm-Nd geochronology of the ophiolites from the SE Turkey: implications for the Neotethyan evolution. Geodinamica Acta 25, 146–161.

Karig, D.E., Kozlu, H., 1990. Late Paleogene-Neogene evolution of the triple junction region near Maraş, South-central Turkey. Journal of the Geological Society London 147, 1023–1034.

Ketin, İ., 1983. Introduction to Geology of Turkey. İstanbul Teknik Üniversitesi Vakfı, İstanbul. Yayın No: 32.

Koglin, N., 2008. Geochemistry, Petrogenesis and Tectonic Setting of Ophiolites and Mafic-ultramafic Complexes in the Northeastern Aegean Region: New Trace-element, Isotopic and Age Constraints. Ph.D thesis. University of Mainz, Germany.

Koglin, N., Kostopoulos, D., Reichmann, T., 2009. Reichmann, Geochemistry, petrogenesis and tectonic setting of the Samothraki mafic suite, NE Greece: trace-element, isotopic and zircon age constraints. Tectonophysics 473, 53–68. https://doi.org/10.1016/j.tecto.2008.10.028.

Komor, S.C., Elthon, D., Casey, J.F., 1985. Mineralogical variations in layered ultramafic cumulate sequences at the North Arm Mountain massif, Bay of Island ophiolite, Newfoundland. Journal of Geophysical Research 90, 7705–7736.

Konstantinou, A., Wirth, K.R., Vervoort, J., 2007. U-Pb isotopic dating of Troodos plagiogranite, Cyprus by LA-ICP-MS. In: Geological Society of America, Annual Meeting, Denver, CO, vol. 28, p. p31.

Kuşçu, I., Gençalioğlu-Kuşçu, G., Tosdal, R.M., Ulrich, T.D., Friedman, R., 2010. Magmatism in the southeastern Anatolian orogenic belt: transition from arc to post-collisional setting in an evolving orogen. Special Publications. In: Sosson, M., Kaymakcı, N., Stephenson, R.A., Bergerat, F., Starostenko, V. (Eds.), Sedimentary Basin Tectonics from the Black Sea and Caucasus to the Arabian Platform, vol. 340. Geological Society, London, Special Publication, pp. 437–460.

Le Bas, N.J., 1962. The role of aluminium in igneous clinopyroxenes with relation to their parentage. Americal Journal of Science 260, 267–288.

Leterrier, J., Maury, R.C., Thonon, P., Girard, D., Marechal, M., 1982. Clinopyroxene composition as a method of identification of the magmatic affinities of paleo-volcanic series. Earth and Planetary Science Letters 59, 139–154.

Liati, A., Gebauer, D., Fanning, M., 2004. The age of ophiolitic rocks of the Hellenides (Vourinos, Pindos, Crete): first U-Pb ion microprobe (SHRIMP) zircon ages. Chemical Geology 207, 171–188.

Medaris Jr., L.G., 1972. High-pressure peridotites in southwestern Oregon. Geological Society of America Bulletin 83, 41–58.

Morimoto, N., Fabries, J., Ferguson, A.K., Ginzburg, I.V., Ross, M., Seifert, F.A., Zussman, J., Aoki, K., Gottardi, D., 1988. Nomenclature of pyroxenes. Americal Mineralogist 62, 53–62.

MTA, 2002. 1/500.000 Scale Geological Map of Turkey. General Directorate of Mineral Research and Exploration, Ankara, Turkey.

Mukasa, S.B., Ludden, J.N., 1987. Uranium-lead ages of plagiogranites from the Troodos ophiolite, Cyprus, and their tectonic significance. Geology 5, 825–828.

Oberhänsli, R., Candan, O., Bousquet, R., Rimmele, G., Okay, A.I., Goff, J., 2010. Alpine HP evolution of the eastern Bitlis complex, SE Turkey. In: Sosson, M., Kaymakci, N., Stephenson, R., Strarostenko, V., Bergerat, F. (Eds.), Sedimentary Basins, Tectonics from Black Sea and Caucasus to the Arabian Platform, vol. 340. Geological Society, London, Special Publications, pp. 461–483.

Okay, A.I., Zattin, M., Cavazza, W., 2010. Apatite fission-track data for the Miocene Arabia-Eurasia collision. Geology 38, 35–38.

Pallister, J.S., Hopson, C.A., 1981. Samail Ophiolite plutonic suite: field relations, phase variation, cryptic variation and layering, and a model of a spreading ridge magma chamber. Journal of Geophysical Research 86 (B4), 2593–2644.

Panjasawatwong, Y., Danyushevsky, L.V., Crawford, A.J., Harris, K.L., 1995. An experimental study of the effects of melt composition on plagioclase-melt equilibria at 5 and 10 kbars: implications for the origin of magmatic high-An plagioclase. Contributions to Mineralogy and Petrology 118, 420–432.

Parlak, O., 2006. Geodynamic significance of granitoid magmatism in the southeast Anatolian orogen: geochemical and geochronogical evidence from Göksun–Afşin (Kahramanmaras, Turkey) region. International Journal of Earth Sciences 95, 609–627.

Parlak, O., Delaloye, M., Bingöl, E., 1996. Mineral chemistry of ultramafic and mafic cumulates as an indicator of the arc-related origin of the Mersin ophiolite (southern Turkey). Geologische Rundschau 85, 647–661.

Parlak, O., Delaloye, M., Bingöl, E., 1997. Phase and cryptic variation through the ultramafic and mafic cumulates in the Mersin ophiolite (southern Turkey). Ofioliti 22 (1), 81–92.

Parlak, O., Höck, V., Delaloye, M., 2000. Supra-subduction zone origin of the Pozantı-Karsantı ophiolite (southern Turkey) deduced from whole-rock and mineral chemistry of the gabbroic cumulates. In: Bozkurt, E., Winchester, J.A., Piper, J.D.A. (Eds.), Tectonics and Magmatism in Turkey and the Surroundings Area, vol. 173. Geological Society, London, Special Publications, pp. 219–234.

Parlak, O., Höck, V., Delaloye, M., 2002. The supra-subduction zone Pozantı-Karsantı ophiolite, southern Turkey: evidence for high-pressure crystal fractionation of ultramafic cumulates. Lithos 65, 205–224.

Parlak, O., Höck, V., Kozlu, H., Delaloye, M., 2004. Oceanic crust generation in an island arc tectonic setting, SE Anatolian Orogenic Belt (Turkey). Geological Magazine 141, 583–603.

Parlak, O., Karaoğlan, F., Rızaoğlu, T., Klotzli, U., Koller, F., Billor, Z., 2013a. U–Pb and ^{40}Ar-^{39}Ar geochronology of the ophiolites and granitoids from the Tauride belt: implications for the evolution of the Inner Tauride suture. Journal of Geodynamics 65, 22–37.

Parlak, O., Karaoğlan, F., Rızaoğlu, T., Nurlu, N., Bağcı, U., Höck, V., Önal Öztüfekçi, A., Kürüm, A., Topak, Y., 2013b. Petrology of the İspendere (Malatya) ophiolite from the southeast Anatolia: implications for the late mesozoic evolution of the southern Neotethyan ocean. In: Robertson, A.H.F., Parlak, O., Ünlügenç, U.C. (Eds.), Geological Development of Anatolia and the Easternmost Mediterranean Region, vol. 372. Geological Society, London, Special Publication, pp. 219–247.

Parlak, O., Rızaoğlu, T., Bağcı, U., Karaoğlan, F., Höck, V., 2009. Tectonic significance of the geochemistry and petrology of ophiolites in southeast Anatolia, Turkey. Tectonophysics 473, 173–187.

Parlak, O., Yılmaz, H., Boztuğ, D., 2006. Geochemistry and tectonic setting of the metamorphic sole rocks and isolated dykes from the Divriği ophiolite (Sivas, Turkey): evidence for melt generation within an asthenospheric window prior to ophiolite emplacement. Turkish Journal of Earth Sciences 15, 25–45.

Pearce, J.A., Norry, M.J., 1979. Petrogenetic implications of Ti, Zr, Y, and Nb variations in volcanic rocks. Contributions to Mineralogy and Petrology 69, 33–47.

Pearce, J.A., van der Laan, S.R., Arculus, R.J., Murton, B.J., Ishii, T., Peate, D.W., Parkinson, I.J., 1992. Boninite and harzburgite from Leg 125 (Bonin-Mariana forearc): a case study of magma genesis during the initial stages of subduction. In: Fryer, P., Pearce, J.A., Stokking, L.B., et al. (Eds.), Proceeding of the Ocean Drilling Program, Scientific Results, vol. 125, pp. 623–659.

Perinçek, D., Kozlu, H., 1984. Stratigraphical and structural relations of the units in the Afşin-Elbistan-Doğanşehir region (Eastern Taurus). In: Tekeli, O., Göncüoğlu, M.C. (Eds.), Geology of the Taurus Belt. Proceedings of International Symposium. MTA, Ankara, pp. 181–198.

Reagan, M.K., Ishizuka, O., Stern, R.J., Kelley, K.A., Ohara, Y., Blichert-Toft, J., Bloomer, S.H., Cash, J., Fryer, P., Hanan, B.B., Hickey-Vargas, R., Ishii, T., Kimura, J.I., Peate, D.W., Rowe, M.C., Woods, M., 2010. Forearc basalts and subduction initiation in the Izu-Bonin Mariana system. Geochemistry Geophysics Geosystems 11, Q03X12. https://doi.org/10.1029/2009GC002871.

Rızaoğlu, T., Parlak, O., Höck, V., İşler, F., 2006. Nature and significance of Late Cretaceous ophiolitic rocks and its relation to the Baskil granitoid in Elazığ region, SE Turkey. In: Robertson, A.H.F., Mountrakis, D. (Eds.), Tectonic Development of the Eastern Mediterranean, vol. 260. Geological Society, London, Special Publication, pp. 327–350.

Rızaoğlu, T., Parlak, O., Höck, V., Koller, F., Hames, W.E., Billor, Z., 2009. Andean type active margin formation in the Eastern Taurides: geochemical and geochronological evidence from the Baskil Granitoid, SE Turkey. Tectonophysics 473, 188–207.

Robertson, A.H.F., 1986a. The Hatay ophiolite (southern Turkey) in its eastern Mediterranean tectonic context: a report on some aspects of the field excursion. Ofioliti 11, 105–119.

Robertson, A.H.F., 1986b. Geochemistry and tectonic implications of metalliferous and volcanoclastic sedimentary rocks associated with late Cretaceous ophiolitic extrusives in the Hatay area, southern Turkey. Ofioliti 11, 121–140.

Robertson, A.H.F., 2002. Overview of the genesis and emplacement of Mesozoic ophiolites in the eastern Mediterranean Tethyan region. Lithos 65, 1–67.

Robertson, A.H.F., Parlak, O., Ustaömer, T., Taslı, K., İnan, N., Dumitrica, P., Karaoğlan, F., 2013a. Subduction, ophiolite genesis and collision history of Tethys adjacent to the Eurasiancontinental margin: new evidence from the Eastern Pontides, Turkey. Geodinamica Acta 26 (3–4), 230–293.

Robertson, A.H.F., Parlak, O., Metin, Y., Vergili, Ö., Taslı, K., İnan, N., Soycan, H., 2013b. Late Palaeozoic-Cenozoic tectonic development of carbonate platform, margin and oceanic units in the Eastern Taurides, Turkey. In: Robertson, A.H.F., Parlak, O., Ünlügenç, U.C. (Eds.), Geological Development of Anatolia and the Easternmost Mediterranean Region, vol. 372. Geological Society, London, Special Publication, pp. 167–218.

Robertson, A.H.F., Parlak, O., Rızaoğlu, T., Ünlügenç, U.C., İnan, N., Taslı, K., Ustaömer, T., 2007. Tectonic evolution of the south Tethyan Ocean: evidence from the eastern Taurus mountains (Elazığ region, SE Turkey). In: Ries, A.C., Butler, R.W.H., Graham, R.H. (Eds.), Deformation of the Continental Crust: The Legacy of Mike Coward, vol. 272. Geological Society, London, Special Publication, pp. 231–270.

Robertson, A.H.F., Parlak, O., Ustaömer, T., 2012. Overview of the palaeozoic-neogene evolution of Neotethys in the eastern Mediterranean region (S Turkey, Cyprus, Syria). Petroleum Geosciences 18, 381–404.

Robertson, A.H.F., Ustaömer, T., Parlak, O., Ünlügenç, U.C., Taslı, K., İnan, N., 2006. The Berit transect of the Tauride thrust belt, S. Turkey: late Cretaceous-Early Cenozoic accretionary/collisional processes related to closure of the southern Neotethys. Journal of Asian Earth Sciences 27, 108–145.

Ross, C.S., Foster, M.D., Myers, A.T., 1954. Origin of dunites and olivine rich inclusions in basaltic rocks. American Mineralogist 39, 693–737.

Saccani, E., Allahyari, K., Beccaluva, L., Bianchini, G., 2013. Geochemistry and petrology of the Kermanshah ophiolites (Iran): implication for the interaction between passive rifting, oceanic accretion, and OIB-type components in the southern Neo-Tethys Ocean. Gondwana Research 24, 392–411.

Saccani, E., Allahyari, K., Rahimzadeh, B., 2014. Petrology and geochemistry of mafic magmatic rocks from the Sarve-Abad ophiolites (Kurdistan region, Iran): evidence for interaction between MORB-type asthenosphere and OIB-type components in the southern Neo-Tethys Ocean. Tectonophysics 621, 132–147.

Sarıfakıoğlu, E., Dilek, Y., Uysal, I., 2012. The petrogenesis and geodynamic significance of Bahçe (Osmaniye) ophiolite. In: 5th Geochemistry Symposium, pp. 112–113. Abstracts.

Sharaskin, A.Y., Migdisov, A.A., Rostchina, I.A., Miklishansky, A.Z., 1983. Major and Trace Element Chemistry of Hole 504B, Basalts and their Alteration Products (Costa Pica Rift, Deep Sea Drilling Project Leg 70). Initial Reports of the Deep Sea Drilling Project, vol. 69, pp. 775–790.

Sisson, T.W., Grove, T.L., 1993. Experimental investigations of the role of H_2O in calc-alkaline differentiation and subduction zone magmatism. Contributions to Mineralogy and Petrology 113, 143–166.

Stern, R.J., 1979. On the origin of andesite in the northern Mariana island arc: implications for agrigan. Contributions to Mineralogy and Petrology 68, 207–219.

Stern, R.J., Bloomer, S.H., 1992. Subduction zone infancy: examples from the Eocene Izu-Bonin-Mariana and Jurassic California arcs. Bulletin of Geological Society of America 104, 1621–1636.

Takagi, D., Sato, H., Nakagawa, M., 2005. Experimental study of a low-alkali tholeiite at 1-5 kbar: optimal condition for the crystallization of high-An plagioclase in hydrous arc tholeiite. Contributions to Mineralogy and Petrology 149, 527–540.

Tarhan, N., 1986. Geology of Göksun-Afşin-Elbistan regions. Jeoloji Mühendisliği 19, 3–9.

Taylor, B., 1992. Rifting and the volcanic-tectonic evolution of the Izu-Bonin-Mariana arc. In: Taylor, B., Fujioka, K., et al. (Eds.), Proceedings of the Ocean Drilling Program, Scientific Results, pp. 627–651.

Tekeli, O., Erendil, M., 1986. Geology and petrology of the Kızıldağ ophiolite (Hatay). Bulletin of Mineral Research and Exploration Institute of Turkey 21, 21–37.

Thy, P., Schiffman, P., Moores, E.M., 1989. Igneous mineral stratigraphy and chemistry of the Cyprus Crustal Study Project drill core in the plutonic sequences of the Troodos Ophiolite. Geological Survey of Canada Paper 88 (9), 147–185.

Topuz, G., Göçmengil, G., Rolland, Y., Çelik, Ö.F., Zack, T., Schmitt, A.K., 2012. Jurassic accretionary and ophiolite from northeast Turkey: No evidence for the Cimmerian continental ribbon. Geology 41, 255–258. https://doi.org/10.1130/G33577.1.

Uysal, İ., Dokuz, A., Kapsiotis, A., Saka, S., Karsli, O., Kaliwoda, M., 2017. Petrogenesis of ultramafic rocks from the eastern Orhaneli ophiolite, NW Turkey: hints on the initiation and evolution of melt-peridotite interaction processes within a heterogeneously depleted mantle section. Journal of Asian Earth Sciences 148, 51–64.

Uysal, İ., Ersoy, E.Y., Dilek, Y., Escayola, M., Sarıfakıoğlu, E., Saka, S., Hirata, T., 2015. Depletion and refertilization of the Tethyan oceanic upper mantle as revealed by the early Jurassic Refahiye ophiolite, NE Anatolia-Turkey. Gondwana Research 27, 594–611.

Uysal, İ., Ersoy, E.Y., Karslı, O., Dilek, Y., Sadıklar, M.B., Ottley, C.J., Tiepolo, M., Meisel, T., 2012. Coexistence of abyssal and ultra-depleted SSZ type mantle peridotites in a Neo-Tethyan ophiolite in SW Turkey: constraints from mineral composition, whole-rock geochemistry (major-trace-REE-PGE), and Re-Os isotope systematics. Lithos 132, 50–69.

van Hinsbergen, D.J., Maffione, M., Plunder, A., Kaymakci, N., Ganerød, M., Hendriks, B.W.H., Corfu, F., Gürer, D., de Gelder, G.I.N.O., Peters, K., McPhee, P.J., Brouwer, F.M., Advokaat, E.L., Vissers, R.L.M., 2016. Tectonic evolution and paleogeography of the Kırşehir block and the central Anatolian ophiolites, Turkey. Tectonics 35, 983–1014.

Yazgan, E., Chessex, R., 1991. Geology and tectonic evolution of the southeastern Taurides in the region of Malatya. Turkish Association of Petroleum Geologists 3, 1–42.

Yılmaz, Y., 1990. Comparison of young volcanic associations of western and eastern Anatolia formed under a compressional regime: a review. Journal of Volcanology and Geothermal Research 44, 69–87.

Yılmaz, Y., 1993. New evidence and model on the evolution of the Southeast Anatolian orogen. Bulletin of Geological Society of America 105, 251–271.

Yılmaz, Y., Şaroğlu, F., Günay, Y., 1987. Initation of the neomagmatism in east Anatolia. Tectonophysics 137, 177–199.

Yılmaz, Y., Yiğitbaş, E., Genç, Ş.C., 1993. Ophiolitic and metamorphic assemblages of southeast Anatolia and their significance in the geological evolution of the orogenic belt. Tectonics 12, 1280–1297.

Yoder, H.S., 1969. Calc-alkaline andesites: experimental data bearing the origin of assumed characteristics. In: McBirney, A.R. (Ed.), Proceedings of Andesite Conference, vol. 65. Oregon University Department of Geology Mineral Industry Bulletin, pp. 43–64.